

# Bayesian Modeling of Microbiome Data for Differential Abundance Analysis

Qiwei Li \*<sup>1</sup>, Shuang Jiang\*<sup>2, 4</sup>, Andrew Y. Koh<sup>3</sup>, Guanghua Xiao<sup>†4</sup> and  
Xiaowei Zhan<sup>†4</sup>

<sup>1</sup>Center for Depression Research and Clinical Care, University of Texas  
Southwestern Medical Center

<sup>2</sup>Department of Statistical Science, Southern Methodist University

<sup>3</sup>Departments of Pediatrics and Microbiology, University of Texas  
Southwestern Medical Center

<sup>4</sup>Quantitative Biomedical Research Center, Department of Population  
and Data Sciences, University of Texas Southwestern Medical Center

## Abstract

The advances of next-generation sequencing technology have accelerated study of the microbiome and stimulated the high throughput profiling of metagenomes. The

---

\*These authors contributed equally to this work.

<sup>†</sup>To whom correspondence should be addressed.

large volume of sequenced data has encouraged the rise of various studies for detecting differentially abundant taxonomic features across healthy and diseased populations, with the ultimate goal of deciphering the relationship between the microbiome diversity and health conditions. As the microbiome data are high-dimensional, typically featuring by uneven sampling depth, overdispersion and a huge amount of zeros, these data characteristics often hamper the downstream analysis. Moreover, the taxonomic features are implicitly imposed by the phylogenetic tree structure and often ignored. To overcome these challenges, we propose a Bayesian hierarchical modeling framework for the analysis of microbiome count data for differential abundance analysis. Under this framework, we introduce a bi-level Bayesian hierarchical model that allows a flexible choice of the count generating process, and hyperpriors in the feature selection scheme. We particularly focus on employing a zero-inflated negative binomial model with a Bayesian nonparametric prior model on the bottom level, and applying Gaussian mixture models for differentially abundant taxa detection on the top level. Our method allows for the simultaneous modeling of sample heterogeneity and detecting differentially abundant taxa. We conducted comprehensive simulations and summarized the improved statistical performances of the proposed model. We applied the model in two real microbiome study datasets and successfully identified biologically validated differentially abundant taxa. We hope that the proposed framework and model can facilitate further microbiome studies and elucidate disease etiology.

*Keywords:* Bayesian hierarchical model; Count data; Feature selection; Microbiome; Mixture models.

# 1 Introduction

A human body hosts more than 10 trillions of microorganisms, whose collective genome contains at least 100 times as many genes as the human genome (Bäckhed et al. 2005). The microbes in a healthy body can maintain digestion and metabolism, and prevent the colonization of pathogenic microorganisms (Honda & Littman 2012). However, an impaired microbiome has been found to be associated with diseases such as liver cirrhosis, schizophrenia, (Zeller et al. 2014, Castro-Nallar et al. 2015). Detection of the association and exploration of the causality of microbiota-associated diseases can facilitate the elucidation of disease etiology and the development of novel treatments.

The advances of next-generation sequencing technology have accelerated the microbiome study by generating an enormous amount of sequencing data at low cost (Metzker 2010). This technology can profile metagenomes in high-throughput sequencing (Ansorge 2009). The availability of big data further motivates the methodology research to focus on the detection of disease-associated bacteria. Microbiome data has unique characteristics that pose challenges for downstream analyses. For example, the microbiome data are overdispersed count data, and they have a large fraction of missing values (Li 2015). It is common for the counts of a taxon to be mostly zeros cross patients; meanwhile, the non-zero counts can range from a few reads to hundreds of thousands of reads. Thus we want to build a specific model for microbiome data. In particular, this model will provide normalization to enable cross-sample comparisons, and simultaneously, to detect differentially abundant taxa among two or more disease outcomes.

First, we have surveyed normalization methods in the context of sequence data analysis. These methods can handle the varying sequencing depths between samples. Rarefying is a classic normalization method in microbiome analysis, which down-samples the sequence reads of each sample until all samples have an the equal number of total counts. This approach discards many sequence reads and thus reduces statistical power (McMur-

die & Holmes 2014). Other normalization methods often multiply the sequence counts by per-specified values. The multiplier, also known as the size factor, is often calculated directly from the observed data. In this paper, we investigate five common normalization methods. However, although these methods are straightforward to implement, they provide non-optimal performance and limit the power of downstream analysis (McMurdie & Holmes 2014). The reason is that size factors are treated as fixed values, and it is an *ad hoc* decision that has to be made in the analysis step (Bullard et al. 2010, Dillies et al. 2013, Weiss et al. 2017). As a consequence, normalization methods often bias the true “hidden” size factors. To overcome these limitations, we propose a Bayesian non-parametric approach for data normalization. In particular, we impose a stochastic prior for estimating the size factor, which serves to incorporate our uncertainties in modeling huge sample variations, and to allow the heterogeneity in microbiome abundance to be specified in a data-adaptive way.

Second, we want to compare the normalized abundances between samples. This is commonly referred to as differential abundance analysis with the goal of detecting disease-associated microbiota. The detected taxa should have statistically significantly different abundances among disease outcomes (e.g., patients and health controls). A widely-used choice is the nonparametric test (e.g., Wilcoxon rank-sum test) and it is applicable to the fraction of taxa data (known as compositional data ) (La Rosa et al. 2015). Several differential expression analysis methods for RNA-seq data (e.g., DESeq2 (Love et al. 2014) and EdgeR (Robinson et al. 2010) ) are commonly applied for microbiome data analysis due to the similar data types (count data). However, these methods, along with some extensions (Mandal et al. 2015), often fail to account for the excessive zeros in the microbiome data. Recently, parametric models have been proposed to detect microbiota-disease associations. They model the count data in negative binomial or Dirichlet-multinomial distribution to account for overdispersion (Holmes et al. 2012, Paulson et al. 2013, Chen

& Li 2013, Zhang et al. 2017). Zero-inflated (ZI) parametric model are also proposed, and they have advantages in controlling type I error with higher statistical power (Xu et al. 2015). These include the ZI log-normal model Sohn et al. (2015), a ZI negative binomial model Zhang et al. (2016), a ZI Poisson regression model, and a ZI beta regression model (Cheung 2002, Peng et al. 2016). Although these models have improved over time, they have limitations, such as the requirement of a separate normalization step, the inability to jointly test multiple taxa and the inability to naturally support multiple groups. We thus propose a Bayesian approach based on a Gaussian mixture model for differential abundance analysis. Accompanied with the Bayesian stochastic priors for data normalization, we are able to simultaneously detect the differentially abundant taxa for multiple outcomes under the specified false discovery rate.

In all, we will present a general hierarchical framework for differential abundance analysis of microbiome count data. It consists of two levels: one level is a multivariate count variable generating process, and the other level is a Gaussian mixture model with feature selection. Under this framework, we construct a Bayesian hierarchical model. In its first level, a wide-range of statistical methods can be applied to normalize microbiome count data into sample-specific latent relative abundance. We focus on two models, the Dirichlet-multinomial (DM) model and the zero-inflated negative binomial (ZINB) model. Furthermore, for the ZINB model, we apply a Bayesian nonparametric approach to infer the normalized factors that account for the sample to sample variations (i.e. sequencing depth). In the second level, a Gaussian mixture model is used to fit the latent relative abundance of multiple groups across multiple taxa simultaneously. Through comprehensive simulations, we showed that our proposed model has better performance compared with other commonly used approaches. We also analyzed two real microbiome datasets, from a cancer study and a psychiatry study, and detected a number of taxa across taxonomic levels. Most of the taxa detected are supported by the existing biological literature

and the novel findings have the potential to be validated in the future.

We have organized the rest of the article as follows. Section 2 introduces the bi-level modeling framework and the Bayesian hierarchical model with stochastic priors. Section 3 describes posterior inference, including the Markov chain Monte Carlo method. Section 4 presents a comprehensive simulation study, and Section 5 applies the model on two real microbiome studies. Section 6 concludes the article with remarks.

## 2 Model

We present a bi-level Bayesian framework for microbial differential abundance analysis in this section. Section 2.1 introduces two representative count generative models as the first (or bottom) level, while Section 2.2 describes a Gaussian mixture model as the second (or top) level. Figure (1) shows the graphical formulations of the proposed models. Before introducing the major components, we depict the input of our framework as follows.

Let  $\mathbf{Y}$  denote an  $n$ -by- $p$  taxonomic abundance table of  $n$  subjects and  $p$  taxa, with  $y_{ij} \in \mathbb{N}, i = 1, \dots, n, j = 1, \dots, p$  indicating the count of taxon  $j$  observed from subject  $i$ . Note that  $\mathbf{Y}$  can be either generated by either the 16S ribosome RNA gene sequencing or the shotgun metagenomic sequencing. For the sake of simplicity, we assume that the taxonomic features in  $\mathbf{Y}$  are all at the lowest available hierarchical levels (e.g. genus or operational taxonomic unit (OTU) for 16S sequencing data, and species for metagenomic sequencing data). As the count matrix at a higher taxonomic level can be easily summed up from the one at its lower level, we discuss how to integrate information from a phylogenetic tree in Section 2.3. We use an  $n$ -dimensional vector  $\mathbf{z} = (z_1, \dots, z_n)^T$  to allocate the  $n$  subjects into  $K$  different groups (i.e. phenotypes, conditions, etc.), with  $z_i = k, k = 1, \dots, K$  indicating that subject  $i$  belongs to group  $k$ . In addition, we use the following notations throughout this paper. For any  $n$ -by- $p$  matrix  $\mathbf{X}$ , we use

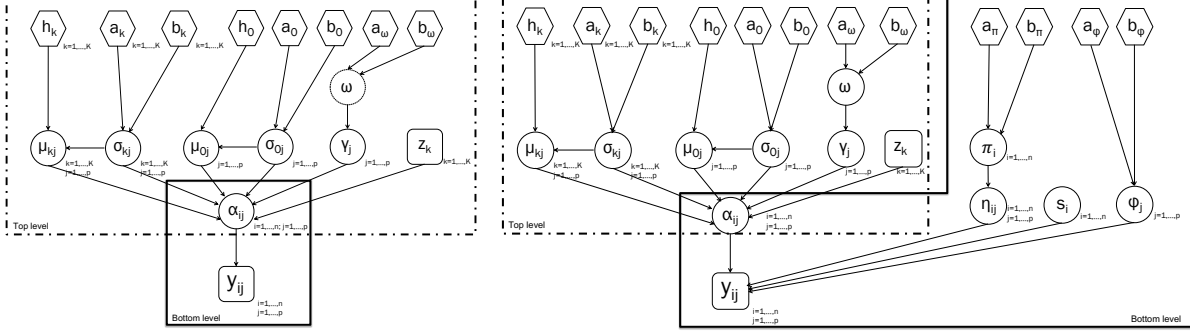


**Figure 1:** A graphical representation of the proposed bi-level Bayesian framework for microbial differential abundance analysis, with the bottom level (within the solid border) of (a) Dirichlet-multinomial (DM) model, and (b) zero-inflated negative binomial (ZINB) model, respectively. Each node in a circle/hexagon/square refers to a model parameter/a fixed hyperparameter/observable data. The link between two nodes represents a direct probabilistic dependence. Note that both (a) and (b) share the same top level (within the dashed border).

$\mathbf{x}_i = (x_{i1}, \dots, x_{ip})^T$  and  $\mathbf{x}_{.j} = (x_{1j}, \dots, x_{nj})^T$  to denote the vector from  $i$ -th row and  $j$ -th column of  $\mathbf{X}$ , respectively, and use  $X_i = \sum_{j=1}^p x_{ij}$  and  $X_{.j} = \sum_{i=1}^n x_{ij}$  to denote the sum of all counts in the  $i$ -th row and  $j$ -th column of  $\mathbf{X}$ , respectively.

## 2.1 Multivariate count variable generating processes

In the bottom level of the proposed framework, we consider that the multivariate counts observed in each subject, denoted by  $\mathbf{y}_i$ , are generated from a probabilistic model  $\mathcal{M}$ . It models the relative abundance of each taxon, and characterizes one or more distinctive attributes of microbiome count data, including uneven sampling depth, zero-inflation, and overdispersion. One advantage of modeling counts via a probabilistic model is that it automatically accounts for measurement errors and other uncertainties associated with the counts (Li 2015). Without loss of generality, we write

$$\mathbf{y}_i \sim \mathcal{M}(\boldsymbol{\alpha}_i, \boldsymbol{\Theta}), \quad (1)$$

where the non-negative vector  $\boldsymbol{\alpha}_i = (\alpha_{i1}, \dots, \alpha_{ip})^T, \alpha_{ij} > 0$  denotes the latent relative abundance for each taxon in subject  $i$ , and  $\boldsymbol{\Theta}$  denotes all other model parameters. A list

of  $\mathcal{M}$  candidates and their characteristics are summarized in Table 1, two of which are discussed in detail as follows.

**Table 1:** A list of multivariate count generating processes and their characterizations

	$\mathcal{M}(\mathbf{y}_i; \boldsymbol{\alpha}_i, \boldsymbol{\Theta})$	Uneven depth	Zero- inflation	Over- dispersion	Example
Multi	Multi( $\mathbf{y}_i; Y_i, \alpha_{i1}, \dots, \alpha_{ip}$ )	•			
DM	DM( $\mathbf{y}_i; \alpha_{i1}, \dots, \alpha_{ip}$ )	•		•	La Rosa et al. (2012)
Poi	$\prod_{j=1}^p \text{Poi}(y_{ij}; s_i \alpha_{ij})$	•			Brown et al. (2011)
NB	$\prod_{j=1}^p \text{NB}(y_{ij}; s_i \alpha_{ij}, \phi_j)$	•		•	Zhang et al. (2017)
ZIG	$\prod_{j=1}^p \pi_i(Y_i) \text{I}(y_{ij} = 0) +$ $(1 - \pi_i(Y_i)) \text{N}(\log(y_{ij} + 1); \alpha_j, \sigma_j^2)$	•	•	•	Paulson et al. (2013)
ZIP	$\prod_{j=1}^p \pi_i \text{I}(y_{ij} = 0) +$ $(1 - \pi_i) \text{Poi}(y_{ij}; s_i \alpha_{ij})$	•	•		Cheung (2002)
ZINB	$\prod_{j=1}^p \pi_i \text{I}(y_{ij} = 0) +$ $(1 - \pi_i) \text{NB}(y_{ij}; s_i \alpha_{ij}, \phi_j)$	•	•	•	Fang et al. (2016)

<sup>1</sup>Abbreviations: Multi is Multinomial, DM is Dirichlet-multinomial, Poi is Poisson, NB is negative binomial, ZIG is zero-inflated Gaussian, ZIP is zero-inflated Poisson, and ZINB is zero-inflated negative binomial.

### 2.1.1 Dirichlet-multinomial model

One commonly used candidate of  $\mathcal{M}$  is the Dirichlet-multinomial (DM) model (see e.g. La Rosa et al. 2012, Holmes et al. 2012, Chen & Li 2013, Wadsworth et al. 2017). To illustrate the model, we start by modeling the taxonomic counts observed in subject  $i$  with a multinomial distribution  $\mathbf{y}_i | \boldsymbol{\psi}_i \sim \text{Multi}(Y_i, \boldsymbol{\psi}_i)$ . The  $p$ -dimensional vector  $\boldsymbol{\psi}_i = (\psi_{i1}, \dots, \psi_{ip})^T$  is defined on a  $p$ -dimensional simplex (i.e.  $\psi_{ij} \geq 0, \forall j$  and  $\sum_{j=1}^p \psi_{ij} = 1$ ), and represents the underlying taxonomic abundances. The probability mass function of the multinomial distribution is  $Y_i \cdot \prod_{j=1}^p \psi_{ij}^{y_{ij}} / y_{ij}!$ , with the mean and variance of each component,  $E(Y_{ij}) = \psi_{ij} Y_i$  and  $\text{Var}(Y_{ij}) = \psi_{ij}(1 - \psi_{ij}) Y_i$ , respectively.



We further impose a Dirichlet prior on the multinomial parameter vector to allow for over-dispersed distributions,  $\boldsymbol{\psi}_i|\boldsymbol{\alpha}_i \sim \text{Dir}(\boldsymbol{\alpha}_i)$ , where each element of the  $p$ -dimensional vector  $\boldsymbol{\alpha}_i = (\alpha_{i1}, \dots, \alpha_{ip})^T$  is strictly positive. Due to the conjugacy between the Dirichlet distribution and the multinomial distribution, we can integrate  $\boldsymbol{\psi}_i$  out,  $p(\mathbf{y}_i|\boldsymbol{\alpha}_i) = \int p(\mathbf{y}_i|\boldsymbol{\psi}_i)p(\boldsymbol{\psi}_i|\boldsymbol{\alpha}_i)d\boldsymbol{\psi}_i$ , resulting in a DM model (Mosimann 1962),

$$\mathbf{y}_i|\boldsymbol{\alpha}_i \sim \text{DM}(\boldsymbol{\alpha}_i), \quad (2)$$

with the probability mass function,

$$f_{\text{DM}}(\mathbf{y}_i|\boldsymbol{\alpha}_i) = \frac{\Gamma(Y_i + 1)\Gamma(A_i)}{\Gamma(Y_i + A_i)} \prod_{j=1}^p \frac{\Gamma(y_{ij} + \alpha_{ij})}{\Gamma(y_{ij} + 1)\Gamma(\alpha_{ij})}. \quad (3)$$

The variance of each count variable is  $\text{Var}(Y_{ij}) = (Y_i + A_i)/(1 + A_i)\text{E}(\psi_{ij})(1 - \text{E}(\psi_{ij}))Y_i$ . Comparing this with the multinomial model, we see that the variation of the DM component is inflated by a factor of  $(Y_i + A_i)/(1 + A_i)$ . Thus, the DM distribution can explicitly model extra variation. Note that  $A_i = \sum_{j=1}^p \alpha_{ij}$  controls the degree of over-dispersion. A small value of  $A_i$  results in large over-dispersion, while a large value approaching infinity essentially reduces the DM model to a multinomial model.

### 2.1.2 Zero-inflated negative binomial model

Although the DM model offers more flexibility than the multinomial model in terms of modeling over-dispersion, neither models accounts for zero-inflation. The excessive zeros are usually caused by that some rare species existing in only a small percentage of samples, whereas others are not recorded owing to the limitations of the sampling effort. Thus we consider modeling each taxonomic count using a zero-inflated negative binomial (ZINB) model,

$$y_{ij} \sim \pi_i \mathbf{I}(y_{ij} = 0) + (1 - \pi_i) \text{NB}(\lambda_{ij}, \phi_j), \quad (4)$$

where we constrain one of the two mixture kernels to be degenerate at zero, thereby allowing for zero-inflation. In model (4),  $\pi_i \in [0, 1]$  can be viewed as the proportion of

extra zero counts in sample  $i$ . We use  $\text{NB}(\lambda, \phi)$ ,  $\lambda, \phi > 0$  to denote a negative binomial (NB) distribution, with expectation  $\lambda$  and dispersion  $1/\phi$ . With this parameterization of the NB model, the probability mass function is written as  $\frac{\Gamma(y+\phi)}{y!\Gamma(\phi)} \left(\frac{\phi}{\lambda+\phi}\right)^\phi \left(\frac{\lambda}{\lambda+\phi}\right)^y$ , with the variance  $\text{Var}(Y) = \lambda + \lambda^2/\phi$ . Note that  $\phi$  controls the degree of over-dispersion. A small value indicates a large variance to mean ratio, while a large value approaching infinity reduces the NB model to a Poisson model with the same mean and variance. Now we rewrite model (4) by introducing a latent indicator variable  $\eta_{ij}$ , which follows a Bernoulli distribution with parameter  $\pi_i$ , such that if  $\eta_{ij} = 1$  then  $y_{ij} = 0$ , whereas if  $\eta_{ij} = 0$  then  $y_{ij} \sim \text{NB}(\lambda_{ij}, \phi_j)$ . The independent Bernoulli prior assumption can be further relaxed by formulating a  $\text{Be}(a_\pi, b_\pi)$  hyperprior on  $\pi_i$ , leading to a beta-Bernoulli prior of  $\eta_{ij}$  with expectation  $a_\pi/(a_\pi + b_\pi)$ . Setting  $a_\pi = b_\pi = 1$  results in a non-informative prior on  $\pi_i$ . Lastly, we specify the same prior distribution for each dispersion parameter as  $\phi_j \sim \text{Ga}(a_\phi, b_\phi)$ . Small values for the two hyperparameters, such as  $a_\phi = b_\phi = 0.001$ , result in a weakly informative gamma prior.

Multiplicative characterizations of the NB (or Poisson as a special case) mean are typical in both the frequentist (e.g., Witten 2011, Li et al. 2012, Cameron & Trivedi 2013) and the Bayesian literature (e.g., Banerjee et al. 2014, Airolidi & Bischof 2016) to justify latent heterogeneity and over-dispersion in multivariate count data. Here, we parameterize the location parameter of the NB distribution as the multiplicative effect of two parameters,  $\lambda_{ij} = s_i \alpha_{ij}$ . We denote  $s_i$  as the size factor of sample  $i$ , reflecting the fact that samples may be sequenced in different depths. Once this global effect is accounted for,  $\alpha_{ij}$  is interpreted as the normalized abundance for counts  $y_{ij}$ . Conditional on the aforementioned parameters, the likelihood of observing the counts  $\mathbf{y}_i$  can be written as

$$f_{\text{ZINB}}(\mathbf{y}_i | \boldsymbol{\alpha}_i, \boldsymbol{\eta}_i, \boldsymbol{\phi}, s_i) = \prod_{j=1}^p \mathbb{I}(y_{ij} = 0)^{\eta_{ij}} \left( \frac{\Gamma(y_{ij} + \phi_j)}{y_{ij}! \Gamma(\phi_j)} \left( \frac{\phi_j}{s_i \alpha_{ij} + \phi_j} \right)^{\phi_j} \left( \frac{s_i \alpha_{ij}}{s_i \alpha_{ij} + \phi_j} \right)^{y_{ij}} \right)^{1 - \eta_{ij}}. \quad (5)$$

To ensure the identifiability between the latent relative abundance  $\alpha_{ij}$  and its relevant

**Table 2:** List of commonly used normalization techniques for count data

	Definition	Constraint	Reference
TSS	$\hat{s}_i \propto Y_i.$	$\sum_{i=1}^n \log s_i = 0$	
Q75	$\hat{s}_i \propto q_i^{0.75p},$	$\sum_{i=1}^n \log s_i = 0$	Bullard et al. (2010)
RLE	$\hat{s}_i \propto \text{median}_j \left\{ y_{ij} / \sqrt{\prod_{i'=1}^n y_{i'j}} \right\}$	$\sum_{i=1}^n \log s_i = 0$	Anders & Huber (2010)
TMM	$\hat{s}_i \propto \sum_{j=1}^p y_{ij} \cdot \exp \left( \frac{\sum_{i \in G^*} \psi_j(i,r) M_j(i,r)}{\sum_{j \in G^*} \psi_j(i,r)} \right)$	$\sum_{i=1}^n \log s_i = 0$	Robinson & Oshlack (2010)
CSS	$\hat{s}_i \propto \sum_{j=1}^p y_{ij} \cdot \mathbf{I}(y_{ij} \leq q_i^{0.5p})$	$\sum_{i=1}^n \log s_i = 0$	Paulson et al. (2013)
DPP	$p(\log s_i   \cdot) = \sum_{m=1}^M \psi_m \left[ t_m \mathbf{N}(\nu_m, \sigma_s^2) + (1 - t_m) \mathbf{N} \left( \frac{c_s - t_m \nu_m}{1 - t_m}, \sigma_s^2 \right) \right]$	$E(\log s_i) = 0$	Li et al. (2017)

<sup>1</sup>Abbreviations: TSS is total sum scaling, Q75 is upper-quartile (i.e. 75%), RLE is relative log expression, TMM is trimmed mean by M-values, CSS is cumulative sum scaling, and DPP is Dirichlet process prior.

<sup>2</sup>Note for Q75 and CSS:  $q_i^l$  is defined as the  $l$ -th quantile of all the counts in sample  $i$ , i.e. there are  $l$  features in sample  $i$  whose values  $y_{ij}$ 's are less than  $q_i^l$ .

<sup>3</sup>Note for TMM: the M-value  $M_j(i, r) = \log(y_{ij}/Y_i) / \log(y_{rj}/Y_r)$  is the log-ratio of scaled counts between sample  $i$  and the reference sample  $r$ , if not within the upper and lower 30% of all the M-values (as well as the upper and lower 5% of all the A-values, defined as  $A_j(i, r) = \log \sqrt{y_{ij}/Y_i \cdot y_{rj}/Y_r}$ , and the corresponding weight  $\psi_{j'}(i, r)$  is the inverse of the approximate asymptotic variances, calculated as  $\frac{Y_i - y_{ij'}}{y_{ij'} Y_i} + \frac{Y_r}{y_{rj'} Y_r}$  by the delta method (Casella & Berger 2002).

size factor  $s_i$ , one typical choice is to estimate  $\mathbf{s} = (s_1, \dots, s_n)$  based on the observed counts  $\mathbf{Y}$ , combined with some constraint such as  $\sum_{i=1}^n s_i = 1$  or  $\prod_{i=1}^n s_i = 1$  (i.e.,  $\sum_{i=1}^n \log s_i = 0$ ). Table 2 summarizes the existing methods for estimating the size factors. The simplest approach is to set the size factor proportional to the total sum of counts in the corresponding sample, i.e.  $\hat{s}_i \propto Y_i$ , although it does not account for heteroscedasticity and yields biased estimation on the other model parameters (Dillies et al. 2013). In practice, most methods have been developed in the context of RNA-Seq data analyses. For example, in order to mitigate the influence of extremely low and high counts on the size factor estimation, Bullard et al. (2010) suggests matching the between-sample distributions in terms of their upper-quartiles (Q75) to normalize the counts from

mRNA-Seq experiments. Furthermore, Anders & Huber (2010) and Robinson & Oshlack (2010) proposed normalization techniques based on relative log expression (RLE) and weighted trimmed mean by M-values (TMM), respectively. Both of them assume that most features (e.g. genes) are not differentially abundant, and of those that are, there is an approximately balanced amount of increased/decreased abundance. However, these assumptions are likely not appropriate for highly diverse microbial environments (Weiss et al. 2017). Witten (2011) compared the clustering performance under different choices of the above size factor inferences with a constraint of  $\sum_{i=1}^n s_i = 1$ . Paulson et al. (2013) have developed a so-called cumulative sum scaling (CSS) method. It is an adaptive extension of Q75, which is better suited for microbiome data. While convenient, the use of plug-in estimates  $\hat{s}_i$ 's has noticeable shortcomings. In a Bayesian framework, those plug-in estimates can be viewed as point mass priors. On one hand, the ‘‘double dipping’’ problem occurs as those informative priors are derived from the data before model fitting and thus the uncertainty quantification for estimation of  $s_i$ 's will not be reflected in the inference; on the other hand, a discontinuity on the point mass priors may introduce bias in model parameter inference. To address the identifiability issue and allow flexibility in the estimation of the unknown normalizing factors  $s_i$ 's, Li et al. (2017) imposed a regularizing prior with a stochastic constraint on the logarithmic scale of each size factor. In particular, it is assumed that  $\log s_i$  is drawn from a mixture of a two-component Gaussian mixture distribution,

$$\log s_i \sim \sum_{m=1}^M \psi_m \left[ t_m \text{N}(\nu_m, \sigma_s^2) + (1 - t_m) \text{N} \left( \frac{c_s - t_m \nu_m}{1 - t_m}, \sigma_s^2 \right) \right], \quad (6)$$

with the weight of outer mixtures denoted by  $\psi_m$  ( $0 \leq \psi_m \leq 1$ ,  $\sum_{m=1}^M \psi_m = 1$ ), and where  $M$  is an arbitrary large positive integer. The use of mixture distributions allows flexible estimation of the posterior density of  $\log s_i$ . In order to satisfy the desired stochastic constraint, each of  $M$  components is further modeled by a mixture of two Gaussian dis-

tributions with a constant mean of  $c_s$ . The weight of each inner mixture is denoted by  $t_m$  ( $0 \leq t_m \leq 1$ ). Note that if  $M \rightarrow \infty$ , model (6) can be interpreted as Bayesian nonparametric infinite mixtures. If we assume the weights  $\psi_m$ 's are defined by the stick-breaking construction, i.e.,  $\psi_1 = V_1, \psi_m = V_m \prod_{u=1}^{m-1} (1 - V_u)$ ,  $m = 1, 2, \dots$ , it becomes a case of Dirichlet process mixture models, which have been extensively used in recent literature for flexible density estimation (see, e.g., Trippa & Parmigiani 2011, Kyung et al. 2011, Taddy & Kottas 2012). Lee & Sison-Mangus (2018) have demonstrated the superiority of employing the Dirichlet process prior (DPP) in a Bayesian semiparametric regression model for joint analysis of ocean microbiome data. It is said that DPP can accommodate various features in a distribution, such as skewness or multi-modality, while satisfying the mean constraint. We conclude the ZINB model by specifying the following hyper-prior distributions for DPP:  $\eta_m \sim \text{Normal}(0, \tau_\eta)$ ,  $t_m \sim \text{Be}(a_t, b_t)$ , and  $V_m \sim \text{Be}(a_m, b_m)$ . Note that  $\psi_m$ 's will be updated according to the stick-breaking construction. We assume that  $\sigma_s^2 = 1$ , which completes an automatic normalization of the size factors.

## 2.2 Gaussian mixture models with feature selection

In the top level of the proposed framework, we aim to identify a subset of taxonomic features that are relevant to discriminate the  $n$  subjects into  $K$  distinct groups. We postulate the existence of a latent binary vector  $\boldsymbol{\gamma} = (\gamma_1, \dots, \gamma_p)^T$ , with  $\gamma_j = 1$  if taxon  $j$  is differentially abundant among the  $K$  groups, and  $\gamma_j = 0$  otherwise. This assumption could be mathematically formulated as,

$$\log \alpha_{ij} | \gamma_j \sim \begin{cases} \text{N}(\mu_{kj}, \sigma_{kj}^2) & \text{if } \gamma_j = 1 \text{ and } z_i = k \\ \text{N}(\mu_{0j}, \sigma_{0j}^2) & \text{if } \gamma_j = 0 \end{cases}. \quad (7)$$

Note that the use of log transformation has two folds: 1) it ensures that the relative abundance  $\alpha_{ij}$ 's are not skewed; 2) it converts a non-negative abundance  $\alpha_{ij}$  to be either

positive or negative, which is more appropriate for Gaussian model fittings. A common choice for the prior of the binary latent vector  $\gamma$  is to assume independent Bernoulli distributions on its individual components with a common hyperparameter  $\omega$ , that is,  $\gamma_j \sim \text{Bernoulli}(\omega)$ . It is equivalent to a binomial prior on the number of discriminatory features; that is,  $p_\gamma = \sum_{j=1}^p \gamma_j \sim \text{Bin}(p, \omega)$ . The hyperparameter  $\omega$  can be elicited as the proportion of taxa expected *a-priori* to be differentially abundant among the  $K$  groups. This prior assumption can be further relaxed by formulating a  $\text{Be}(a_\omega, b_\omega)$  hyperprior on  $\omega$ , which leads to a beta-binomial prior on  $p_\gamma$  with expectation  $pa_\omega/(a_\omega + b_\omega)$ . Tadesse et al. (2005) suggest a vague prior of  $\omega$ , by imposing the constraint  $a_\omega + b_\omega = 2$ . As a result, the desirable mean percentage of inclusion is  $a_\omega/2$ .

Taking a conjugate Bayesian approach, we impose a normal prior on  $\mu_0$  and each  $\mu_k$ , and an inverse-gamma (IG) prior on  $\sigma_0^2$  and each  $\sigma_k^2$ ; that is,

$$\begin{aligned} \mu_{0j} &\sim \text{N}(0, h_0\sigma_0^2), \quad \sigma_{0j}^2 \sim \text{IG}(a_0, b_0) \\ \mu_{kj} &\sim \text{N}(0, h_k\sigma_k^2), \quad \sigma_{kj}^2 \sim \text{IG}(a_k, b_k). \end{aligned} \tag{8}$$

This parametrization setting is standard in most Bayesian normal models. It allows for creating a computationally efficient variable selection algorithm by integrating out means (i.e.  $\mu_0$  and  $\mu_k$ 's) and variances (i.e.  $\sigma_0^2$  and  $\sigma_k^2$ 's). The integration leads to marginal non-standardized Student's t-distributions on  $\log \alpha_{ij}$ 's. Consequently, we can write the likelihood of observing the latent relevant abundances of feature  $j$  as,

$$p(\boldsymbol{\alpha}_{\cdot j} | \gamma_j) = (2\pi)^{-\frac{n}{2}} \times \begin{cases} \prod_{k=1}^K (n_k h_k + 1)^{-\frac{1}{2}} \frac{\Gamma(a_k + \frac{n_k}{2})}{\Gamma(a_k)} \frac{b_k^{a_k}}{\left\{ b_k + \frac{1}{2} \left[ \sum_{\{i: z_i=k\}} \log \alpha_{ij}^2 - \frac{(\sum_{\{i: z_i=k\}} \log \alpha_{ij})^2}{n_k + \frac{1}{h_k}} \right] \right\}^{a_k + \frac{n_k}{2}}} & \text{if } \gamma_j = 1 \\ (nh_0 + 1)^{-\frac{1}{2}} \frac{\Gamma(a_0 + \frac{n}{2})}{\Gamma(a_0)} \frac{b_0^{a_0}}{\left\{ b_0 + \frac{1}{2} \left[ \sum_{i=1}^n \log \alpha_{ij}^2 - \frac{(\sum_{i=1}^n \log \alpha_{ij})^2}{n + \frac{1}{h_0}} \right] \right\}^{a_0 + \frac{n}{2}}} & \text{if } \gamma_j = 0 \end{cases}, \tag{9}$$

where  $n_k$  is the number of subjects belonging to group  $k$ . To specify the IG hyperparameters of  $\sigma_0^2$  and  $\sigma_k^2, k = 1, \dots, K$ , we recommend a weakly informative choice by setting the shape parameters  $a_0$  and  $a_k, k = 1, \dots, K$  to 2, and the scale parameters  $b_0$  and  $b_k, k = 1, \dots, K$  to 1, following Li et al. (2018). To specify the hyperprior on  $h_0$ , we suggest setting it to a large value so as to obtain a fairly flat distribution over the region where the data are defined. According to Stingo et al. (2013), a large value of  $h_k, k = 1, \dots, K$  allows for mixtures with widely different component means and typically encourages the selection of relatively large effects (e.g. those taxa of large effect size among the  $K$  groups), whereas a small value encourages the selection of small effects. We carried out a sensitivity analysis on the simulated data and found that the both the DM and ZINB models perform reasonably well if the value ranges from 10 to 100.

### 2.3 Incorporating the phylogenetic tree

One characteristic of microbiome data is that the count matrix can be summarized in different taxonomic levels, since there is a natural hierarchy of biological organism classification, i.e., species, genus, family, order, class, phylum, and kingdom. Given a count table  $\mathbf{Y}$  at the most bottom level, one can always aggregate the counts into any upper levels based on the phylogenetic tree. A tree is an undirected graph where any two vertices are connected by exactly one path. Thus, we can describe the phylogenetic tree by using the adjacent matrix in graph theory. Suppose the relationship between taxa in different levels are represented in a  $p' \times p'$  symmetric matrix  $\mathbf{G}$ , with  $g_{jj'} = 1$  if taxon  $j$  and  $j'$  have a direct link in the phylogenetic tree. Let  $l, 1 \leq l \leq L$  index the taxonomic level in the order of {1, genus, family, order, class, phylum, kingdom}. Then, given the count matrix in the lower level  $\mathbf{Y}^{(l-1)}$ , each element of the count matrix in the upper level can be calculated by  $y_{ij}^{(l)} = \sum_{\{j': g_{jj'}=1\}} y_{ij'}^{(l-1)}$ .

One property of the DM model is that if  $(y_1, \dots, y_p) \sim \text{DM}(\alpha_1, \dots, \alpha_p)$ , and if any

two random variables, say  $y_j$  and  $y_{j'}$ , are dropped from the vector and replaced by their sum  $y_j + y_{j'}$ , then we have  $(y_1, \dots, y_j + y_{j'}, \dots, y_p) \sim \text{DM}(\alpha_1, \dots, \alpha_j + \alpha_{j'}, \dots, \alpha_p)$ . This aggregation property can be used to derive the abundance matrices in different levels sequentially just from the one at the lowest available level via  $\alpha_{ij}^{(l)} = \sum_{\{j': g_{jj'}=1\}} \alpha_{ij'}^{(l-1)}$ . For a joint analysis supporting the proposed Bayesian framework, we need to: 1) implement the bottom-level model on the microbiome count matrix  $\mathbf{Y}^{(1)}$ , which is at the most bottom level, and infer the corresponding relative abundance matrix  $\mathbf{A}^{(1)}$ ; 2) summarize the abundance matrices at all upper levels,  $\mathbf{A}^{(2)}, \dots, \mathbf{A}^{(L)}$ ; and 3) implement the top-level model on all the abundance matrices from level 1 to  $L$ , independently.

For the ZINB model, the aggregation property does not hold. However, we assume that the size factor estimation should be irrelevant to the choices of microbiome count data at different taxonomic levels. Therefore, we consider the following scheme for a joint analysis: 1) implement the bottom-level model on the microbiome count matrix  $\mathbf{Y}^{(1)}$  and infer the corresponding relative abundance matrix  $\mathbf{A}^{(1)}$ , as well as the sample-specific size factor  $\mathbf{s}$ ; 2) implement the bottom-level model on the microbiome count matrices at all upper levels with fixed values of  $\mathbf{s}$ , and obtain the corresponding relative abundance matrices  $\mathbf{A}^{(l)}$ 's,  $l = 2, \dots, L$ ; and 3) implement the top-level model on all the abundance matrices from level 1 to  $L$ , independently.

### 3 Model Fitting

In this section, we briefly describe the Markov chain Monte Carlo (MCMC) algorithm for posterior inference. Our inferential strategy allows us to simultaneously infer the abundance of each taxon  $j$  (at different taxonomic levels  $l$ ) in each subject  $i$ , while identifying the discriminating taxa through  $\boldsymbol{\gamma}^{(l)}$ 's.



### 3.1 MCMC algorithm

Our primary interest lies in the identification of discriminating taxa via the selection vector  $\boldsymbol{\gamma}^{(l)}$ . Meanwhile, we want to make inference on how multiple subject/patient groups differ with respect to the relative abundance for all discriminatory taxa selected through  $\mathbf{A}^{(l)}$ . To serve this purpose, we design a MCMC algorithm based on Metropolis search variable selection algorithms (George & McCulloch 1997, Brown et al. 1998), which simultaneously selects discriminating taxa and samples the latent relative abundance at different taxonomic levels. The MCMC algorithm is based on our discussion in the second and third paragraphs of Section 2.3. As already shown in Section 2.2, we have integrated out some of the model parameters in the top level, including the variance components in Equation (7) and (8). This step helps us speed up the MCMC convergence and improve the estimation of parameters that we are interested in. We give the major MCMC updates within each iteration as below.

**Update of  $\mathbf{A}^{(1)}$ :** We update each  $\alpha_{ij}^{(1)}, i = 1, \dots, n, j = 1, \dots, p^{(1)}$  sequentially by using a Metropolis-Hastings random walk algorithm. We first propose a new  $\alpha_{ij}^{(1)*}$  from  $N(\alpha_{ij}^{(1)}, \tau_\alpha^2)$ , and then accept the proposed value with probability  $\min(1, m_{\text{MH}})$ , where

$$m_{\text{MH}} = \frac{p(\mathbf{y}_{i\cdot}^{(1)} | \boldsymbol{\alpha}_{i\cdot}^{(1)*}) p(\boldsymbol{\alpha}_{\cdot j}^{(1)*} | \gamma_j^{(1)}) J(\alpha_{ij}^{(1)}; \alpha_{ij}^{(1)*})}{p(\mathbf{y}_{i\cdot}^{(1)} | \boldsymbol{\alpha}_{i\cdot}^{(1)}) p(\boldsymbol{\alpha}_{\cdot j}^{(1)} | \gamma_j^{(1)}) J(\alpha_{ij}^{(1)*}; \alpha_{ij}^{(1)})},$$

where  $J(\cdot|\cdot)$  indicates the proposal probability distribution for the selected move. Note that the proposal density ratio equals 1 here.

**Update of  $(\boldsymbol{\gamma}^{(1)}, \dots, \boldsymbol{\gamma}^{(L)})$ :** This is done conditioned upon  $(\mathbf{A}^{(1)}, \dots, \mathbf{A}^{(L)})$ . We update each  $\gamma_j^{(l)}, j = 1, \dots, p^{(l)}, l = 1, \dots, L$  sequentially via an *add-delete* algorithm. In this approach, a new candidate vector, say  $\boldsymbol{\gamma}^{(l)*}$ , is generated by randomly choosing an element within  $\boldsymbol{\gamma}^{(l)}$ , say  $j$ , and changing its value to  $1 - \gamma_j^{(l)}$ . Then, this proposed move

is accepted with probability  $\min(1, m_{\text{MH}})$ , where the Hastings ratio is

$$m_{\text{MH}} = \frac{p(\boldsymbol{\alpha}_{\cdot j}^{(l)} | \gamma_j^{(l)*}) p(\gamma_j^{(l)*} | \cdot) J(\boldsymbol{\gamma}^{(l)} | \boldsymbol{\gamma}^{(l)*})}{p(\boldsymbol{\alpha}_{\cdot j}^{(l)} | \gamma_j^{(l)}) p(\gamma_j^{(l)} | \cdot) J(\boldsymbol{\gamma}^{(l)*} | \boldsymbol{\gamma}^{(l)})}.$$

Note that the proposal density ratio equals to 1. We should notice that the feature selection and the abundance estimation are determined simultaneously in the MCMC algorithm. Therefore, to improve mixing, it is necessary to allow the selection to stabilize for any visited configurations of  $\mathbf{A}^{(l)}$  and its induced  $\mathbf{A}^{(l)}$ 's. We suggest repeating the above Metropolis step multiple times within each iteration.

### 3.2 Posterior inference

One way to select the discriminating taxa is to use the *maximum-a-posteriori* (MAP) estimates, which is the posterior mode of possible selection results for all taxa considered in the model. However, this is not feasible since usually the total number of taxa is too large. Alternatively, an efficient solution is to select the taxa based on their marginal distributions. In particular, we estimate marginal posterior probabilities of inclusion (PPI) of a single taxon by

$$\text{PPI}_j^{(l)} = \frac{\sum_{b=1}^B (\gamma_j^{(l)} \text{ at iteration } b)}{B},$$

where  $B$  is the total number of iterations after burn-in. Clearly, the marginal PPI represents the proportion of MCMC samples in which a taxon is selected to be discriminatory. A set of differentially abundant taxa can be picked in terms of high PPIs. For example, the selection can be done by including those taxa with marginal PPIs greater than a pre-specified value such as 0.5. Alternatively, we can choose the threshold that controls for multiplicity (Newton et al. 2004), which guarantees the expected Bayesian false discovery

rate (FDR) to be smaller than a number. The Bayesian FDR is calculated as follows,

$$\text{FDR}(c_\gamma) = \frac{\sum_{l=1}^L \sum_{j=1}^p (1 - \text{PPI}_j^{(l)}) \mathbb{I}(1 - \text{PPI}_j^{(l)} < c_\gamma)}{\sum_{l=1}^L \sum_{j=1}^p \mathbb{I}(1 - \text{PPI}_j^{(l)} < c_\gamma)}, \quad (10)$$

where  $c_\gamma$  is the desired significance level. An *a priori* significance level of 0.05 is generally used for interpreting the significance of the result, as in other parametric/nonparametric statistical tests for microbiome studies.

## 4 Simulation

In this section, we use both simulated and synthetic data to assess the performance of the proposed Bayesian framework embedded with the DM and ZINB models, respectively. We also demonstrate the superiority of our models against alternative solutions for the analysis of compositional data and overdispersed count data. Finally, a sensitivity analysis is conducted to investigate how the prior choices affect the posterior inference, which can be found in the supplement.

### 4.1 Generative models

Let  $Y$  denote the microbiome count data sampled according to the generative models as described in Section 4.1.1 and 4.1.2. The dimension of  $Y$  was set to  $n$  and  $p = 1,000$ . With the assumption that there is no hierarchical structure among the  $p$  features, we set the number of truly discriminatory taxonomic features  $p_\gamma = 50$  so as to test the ability of our method to discover relevant features in the presence of a good amount of noise. We considered two scenarios of the sample size,  $n = 24$  or 108. For the set of discriminatory features, we assumed that the relative abundance for each feature can be clustered into  $K = 2$  or 3 homogeneous groups. The hierarchical formulations of the generative models are presented in Table 3.

The proposed DM Model	Simulated data	Synthetic data
<p>The model proposed by Weiss et al. (2017):</p> <p>Count generative model:</p> <p>For <math>i = 1, \dots, n</math></p> $\mathbf{y}_i \sim \text{Multi}(10,000, \boldsymbol{\phi}_i.)$ $\psi_i = \mathbf{I} \left( 1 \leq i \leq \frac{n}{2} \right) \frac{\mathbf{P}}{\sum_{j=1}^p P_j} + \mathbf{I} \left( \frac{n}{2} < i \leq n \right) \frac{\mathbf{Q}}{\sum_{j=1}^p Q_j}$ <p>Abundance generative model:</p> $P_j = \begin{cases} \exp(\sigma)O_j & \text{for } 1 \leq j \leq p_\gamma/2 \\ O_j & \text{otherwise} \end{cases}$ $Q_j = \begin{cases} \exp(\sigma)O_j & \text{for } p_\gamma/2 < j \leq p_\gamma \\ O_j & \text{otherwise} \end{cases}$ $\mathbf{O} = (O_1, \dots, O_{p_\gamma/2}, O_1, \dots, O_{p_\gamma/2}, O_{p_\gamma+1}, \dots, O_p)^T,$ <p>which is summarized from real data</p>	<p>The proposed ZINB Model</p> <p>Bottom level :</p> <p>For <math>i = 1, \dots, n</math></p> $\mathbf{y}_i \sim \text{Multi}(N_i, \boldsymbol{\psi}_i.)$ $N_i \sim \text{U}(5,000, 10,000)$ $\boldsymbol{\psi}_i. \sim \text{Dir}(\boldsymbol{\alpha}_i.)$ <p>For <math>i = 1, \dots, n, j = 1, \dots, p</math></p> $y_{ij} \sim 0.5\text{I}(y_{ij} = 0) + 0.5\text{NB}(s_i \alpha_{ij}, \phi_i)$ $s_i \sim \text{U}(0.5, 4)$ $\phi_j \sim \text{Exp}(1/10)$ <p>Top level:</p> $\log \alpha_{ij} \sim \begin{cases} \mathbf{I} \left( 1 \leq i \leq \frac{n}{2} \right) \text{N} \left( d_{1j}, \sigma^2 \right) + \mathbf{I} \left( \frac{n}{2} < i \leq n \right) \text{N} \left( d_{2j}, \sigma^2 \right), & \text{if } \gamma_j = 1 \text{ and } K = 2 \\ \mathbf{I} \left( 1 \leq i \leq \frac{n}{3} \right) \text{N} \left( d_{1j}, \sigma^2 \right) + \mathbf{I} \left( \frac{n}{3} < i \leq \frac{2n}{3} \right) \text{N} \left( d_{2j}, \sigma^2 \right) + \mathbf{I} \left( \frac{2n}{3} < i \leq n \right) \text{N} \left( d_{3j}, \sigma^2 \right), & \text{if } \gamma_j = 1 \text{ and } K = 3 \\ \text{N}(d_{0j}, \sigma^2/100), & \text{if } \gamma_j = 0 \end{cases}$ $d_{0j} \sim \text{U}(0, 4)$ $\text{sort}(d_{1j}, \dots, d_{Kj}) = \begin{cases} (1 - \sigma/2, 1 + \sigma/2), & \text{if } K = 2 \\ (1 - \sigma, 1, 1 + \sigma), & \text{if } K = 3 \end{cases}$	

**Table 3:** Hierarchical formulations of the data generative models used in the simulation study. Note that the sample size  $n \in \{24, 108\}$ , the number of features  $p = 1,000$  with 50 discriminating among  $K$  groups ( $K \in \{2, 3\}$  for simulated data and  $K = 2$  for synthetic data), and the effect size  $\sigma \in \{1, 2\}$ .

### 4.1.1 Generating simulated data

The simulated datasets were generated by the proposed bi-level Bayesian frameworks with the same top level. In particular, for the relative abundance  $\alpha_{ij}$  in a discriminating feature (i.e.  $\gamma_j = 1$ ), we drew its logarithmic value from a two-component Gaussian mixture distribution,

$$\log \alpha_{ij} | \gamma_j = 1 \sim \text{I} \left( 1 \leq i \leq \frac{n}{2} \right) \text{N} (d_{1j}, \sigma_{\text{within}}^2) + \text{I} \left( \frac{n}{2} < i \leq n \right) \text{N} (d_{2j}, \sigma_{\text{within}}^2)$$

if  $K = 2$ , or a three-component Gaussian mixture distribution,

$$\begin{aligned} \log \alpha_{ij} | \gamma_j = 1 \sim & \text{I} \left( 1 \leq i \leq \frac{n}{3} \right) \text{N} (d_{1j}, \sigma_{\text{within}}^2) + \text{I} \left( \frac{n}{3} < i \leq \frac{2n}{3} \right) \text{N} (d_{2j}, \sigma_{\text{within}}^2) \\ & + \text{I} \left( \frac{2n}{3} < i \leq n \right) \text{N} (d_{3j}, \sigma_{\text{within}}^2) \end{aligned}$$

if  $K = 3$ . Here, each permutation of  $\{d_{1j}, \dots, d_{Kj}\}$  follows an arithmetic progression with unit mean and difference  $\sigma$ . For the scenario of  $K = 2$ ,  $\sigma$  is also known as the between-group standard deviation or the effect size in a logarithmic scale). We considered two scenarios of  $\sigma = 1$  and 2, and set the within-group standard deviation  $\sigma_{\text{within}} = \sigma/10$ . For those non-discriminating features, we generated its logarithmic value from a normal distribution with zero mean and variance 4, i.e.  $\log \alpha_{ij} | \gamma_j = 0 \sim \text{N}(0, 4)$ . For the bottom level of the DM model, we first sampled the underlying fractional abundances for sample  $i$  from a Dirichlet distribution with parameters  $\boldsymbol{\alpha}_i$ , i.e.  $\boldsymbol{\psi}_i \sim \text{Dir}(\boldsymbol{\alpha}_i)$ . Then, the corresponding observed counts  $\mathbf{y}_i$  would be drawn from a multinomial distribution, i.e.  $\text{Multi}(N_i, \boldsymbol{\psi}_i)$ , where the total counts  $N_i$  was randomly selected from a discrete uniform  $\text{U}(50, 000, 10, 000)$ . As for the ZINB model, we independently and identically simulated the size factors  $s_i$ 's from a uniform distribution  $\text{U}(0.5, 4)$ , and the dispersion parameters  $\phi_j$ 's from an exponential distribution with mean 10, i.e.,  $\text{Exp}(1/10)$ . Next, each observed count  $y_{ij}$  would be generated from  $\text{NB}(s_i \alpha_{ij}, \phi_j)$ . Lastly, we randomly forced half of the counts to zero in order to mimic the excess zeros seen in the real data. Combined

with the two bottom-level kernels ( $\{\text{DM, ZINB}\}$ ), and the two choices of the sample size ( $n \in \{24, 108\}$ ), the number of groups ( $K \in \{2, 3\}$ ) and the log effect size ( $\sigma \in \{1, 2\}$ ), there were  $2^4 = 16$  scenarios in total. For each one of the scenarios, we repeated the above steps to generate 50 independent datasets.

#### 4.1.2 Generating synthetic data

To evaluate the performance of the proposed methods on the count data that are different from the model assumptions, we generated synthetic datasets based on multinomial models that characterize a real taxa abundance distribution. A brief description of the data generating scheme is given as below. The detailed information can be found in the supplement of Weiss et al. (2017). Let  $\mathbf{O} = (O_1, \dots, O_{p_\gamma/2}, O_{p_\gamma/2+1}, \dots, O_{p_\gamma}, O_{p_\gamma+1}, \dots, O_p)^T$  be a vector of the observed abundances of  $p - p_\gamma/2$  unique taxa in all samples, where  $(O_1, \dots, O_{p_\gamma/2}) = (O_{p_\gamma/2+1}, \dots, O_{p_\gamma})$ . Each  $O_j, p_\gamma/2 < j \leq p$  is the sum of OTU counts for one randomly selected taxon (without replacement) from all the skin or feces samples in a real microbiome study (Caporaso et al. 2011). Next, we define two  $p$ -by-1 vectors,  $\mathbf{P}$  and  $\mathbf{Q}$ , where

$$P_j = \begin{cases} \exp(\sigma)O_j & \text{for } 1 \leq j \leq p_\gamma/2 \\ O_j & \text{otherwise} \end{cases}, \text{ and } Q_j = \begin{cases} \exp(\sigma)O_j & \text{for } p_\gamma/2 < j \leq p_\gamma \\ O_j & \text{otherwise} \end{cases},$$

where  $\sigma$  represents the effect size in a logarithmic scale. Note that  $\sum_{j=1}^p P_j = \sum_{j=1}^p Q_j$ . The observed counts  $\mathbf{y}_i$  would be drawn from a multinomial model  $\text{Multi}(N_i, \boldsymbol{\psi}_i)$ , where  $N_i = 10,000$  and

$$\boldsymbol{\psi}_i = I\left(1 \leq i \leq \frac{n}{2}\right) \frac{\mathbf{P}}{\sum_{j=1}^p P_j} + I\left(\frac{n}{2} < i \leq n\right) \frac{\mathbf{Q}}{\sum_{j=1}^p Q_j}.$$

This would yield the first  $p_\gamma$  taxa to be truly discriminating between the two equally sized groups. Finally, we permuted the columns of the data matrix,  $\mathbf{Y}$ , to disperse the taxa. Combined with the two types of samples ( $\{\text{Skin, Feces}\}$ ), and the two choices of

the sample size ( $n \in \{24, 108\}$ ) and the log effect size ( $\sigma \in \{1, 2\}$ ), there were  $2^3 = 8$  scenarios in total. For each one of the scenarios, we repeated the above steps to generate 50 independent datasets.

## 4.2 Algorithm settings

For prior specification in the top level of the proposed Bayesian framework, we used the following default settings. We set the hyperparameters that control the selection of discriminatory features,  $\omega \sim \text{Be}(a_\omega = 0.2, b_\omega = 1.8)$ , resulting in the proportion of taxa expected *a-priori* to discriminate among the  $K$  groups to be  $a_\omega / (a_\omega + b_\omega) = 10\%$ . As for the inverse-gamma priors on the variance components  $\sigma_{0j}^2$ 's and  $\sigma_{kj}^2$ 's, we set the shape parameters  $a_0 = a_1 = \dots = a_k = 2$  and the scale parameters  $b_0 = b_1 = \dots = b_k = 1$  to achieve a fairly flat distribution with an infinite variance. We further set the default values of  $h_0$  and  $h_k$ 's to 100, as our sensitivity analysis (presented in the supplement) shows the posterior inference on  $\gamma$  remained almost the same when those values were in the range of 10 to 100. As indicated by Stingo et al. (2013), larger values of these hyperparameters would encourage the selection of only very large effects whereas smaller values would encourage the selection of smaller effects. For the bottom level of the ZINB model, we used the following weakly informative settings. The hyperparameters that control the percentage of extra zeros *a-priori* were set to  $\pi \sim \text{Be}(a_\pi = 1, b_\pi = 1)$ , which is actually a uniform distribution in  $[0, 1]$ . As for the gamma prior on the dispersion parameters, i.e.  $\phi_j \sim \text{Ga}(a_\phi, b_\phi)$ , we set both  $a_\phi$  and  $b_\phi$  to small values such as 0.001, which leads to a vague prior with expectation and variance equal to 1 and 1,000. For the Dirichlet priors on the size factors  $s_i$ 's, we followed Li et al. (2017) by specifying  $M = n/2$ ,  $c_s = 0$ ,  $\sigma_s = 1$ ,  $\tau_\eta = 1$ ,  $a_t = b_t = 1$ , and  $a_m = b_m = 1$ . For each dataset, we ran one MCMC chain described in Section 3.1 with 10,000 iteration and set the first half as burn-in. The chain was initialed from a model with 5% randomly chosen  $\gamma_j$ 's set to 1.

The DM model does not have any parameters needing to be specified in the bottom level.

### 4.3 Performance metrics

To quantify the accuracy of the identification of discriminatory features, via the binary variables  $\gamma$ , by the proposed method, we used two measures of the quality of binary classifications. Both of them are generally regarded as the most appropriate measures of classification accuracy. The first one is the area under the curve (AUC) of the receiver operating characteristic (ROC). This metric considers both true positive (TP) and false positive (FP) rates across various threshold settings. The second one is the Matthews correlation coefficient (MCC) proposed by Matthews (1975), which balances TP, FP, true negative (TN), and false negative (FN) counts even if the true zeros and ones in  $\gamma$  are of very different sizes. MCC is defined as 
$$\text{MCC} = \frac{(\text{TP} \times \text{TN} - \text{FP} \times \text{FN})}{\sqrt{(\text{TP} + \text{FP})(\text{TP} + \text{FN})(\text{TN} + \text{FP})(\text{TN} + \text{FN})}}$$
. In differential analysis settings, the number of truly discriminatory features are usually assumed to be a small fraction to the total. Therefore, MCC is more appropriate to handle such an imbalanced scenario. Note that the AUC yields a value between 0 to 1 that is averaged by all possible thresholds, and the MCC value ranges from  $-1$  to  $1$  to pinpoint a specified threshold. The larger the index, the more accurate the inference.

### 4.4 Results

We first describe posterior inference on the parameters of interest,  $\gamma$  and  $\mathbf{s}$ , on a single simulated dataset generated from the ZINB model. The results were obtained by fitting the proposed framework where the bottom level is a ZINB model with the DPP on  $\log(\mathbf{s}_i)$ . As for the feature selection, Figure 2a shows the marginal PPI of each feature,  $p(\gamma_j|\cdot)$  and the trace plot of the number of selected discriminatory features,  $p_\gamma$ . As shown in Figure 2a, the red dots indicate the truly discriminatory features and the horizontal dashed lines correspond to a threshold that ensures an expected Bayesian FDR of 5%. This



threshold resulted in a model that included 48 features, 43 of which were in the set of truly discriminatory features. As for the size factors  $\mathbf{s}$ , we plot the true values against the estimated ones by different normalization techniques in Figure 2b. It clearly shows that all of the true values were within the 95% credible intervals derived by our method. In other words, the posterior distributions of  $s_i$ 's converged and stabilized around the true values. In comparison, the alternative normalization techniques with constraint  $\prod_{i=1}^n s_i = 1$  yielded biased estimations. One of them, RLE, even failed to produce any result because a large number of zeros is likely to make the geometric means (the key component to calculating the size factors) of a few features inadmissible.

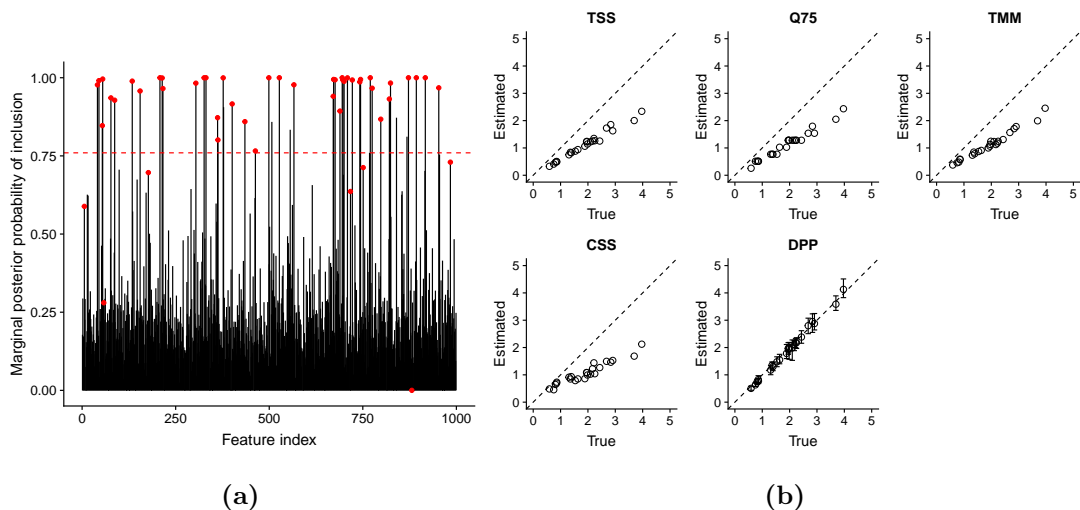


**Figure 2:** Simulated data: (a) Marginal posterior probabilities of inclusion (PPI),  $p(\gamma_j|\cdot)$ , with the red dots indicating truly discriminatory features and the horizontal red dashed line indicating a threshold for a 5% Bayesian FDR; (b) The scatter plots of the true and estimated size factors  $s_i$ 's obtained by different normalization techniques on one of the 50 simulated datasets from the ZINB generative model with  $K = 2$ ,  $n = 24$ , and  $\sigma = 2$ . Note that the proposed ZINB model with DPP can output the estimation uncertainty in terms of the 95% credible interval.

To demonstrate the superiority of the proposed Bayesian models, particularly the ZINB model where the DPP is used to normalize the samples, we compared ours with other general approaches for microbial differential abundance analysis, all of which can be easily implemented in R. They are: 1) Analysis of variance (ANOVA); 2) Kruskal-Wallis

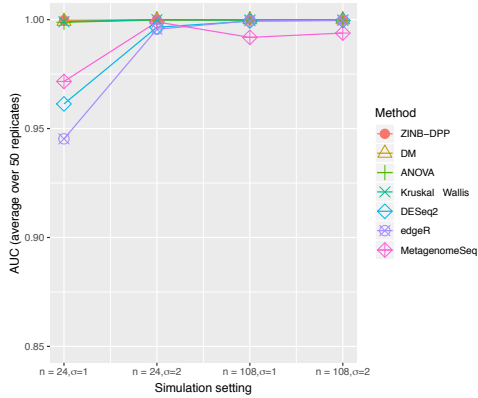
test; 3) `edgeR` (Robinson et al. 2010); 4) `DESeq2` (Love et al. 2014); and 5) `metagenomeSeq` (Paulson et al. 2013). The first two are parametric/nonparametric methods for testing whether samples originate from the same distribution, after converting each  $\mathbf{y}_i$  into a compositional vector of proportions by dividing each count by the total number of reads  $Y_i$ . Note that they aim to determine whether there is a significant difference among the abundance means/medians of multiple groups for each individual taxonomic feature. The third and fourth ones were developed for the analysis of RNA-Seq count data, but can be used to analyze microbiome data (Xia & Sun 2017). `edgeR` implements an exact binomial test generalized for over-dispersed counts, while `DESeq2` employs a Wald test by adopting a generalized linear model based on an NB kernel. The last one, `metagenomeSeq`, assumes a zero inflated Gaussian model on the log-transformed counts, and performs a multiple groups testing on moderated F-statistics. All these competitors produce  $p$ -values. In order to control for the FDR, i.e., the rate of type-I errors in these null hypothesis testings, we further adjusted their  $p$ -values by using the BH method (Benjamini & Hochberg 1995). As mentioned in Section 4.1, we independently generated 50 replicates for each of the 16 simulated data scenarios, and each of the 8 synthetic data scenarios. For each dataset, we ran our methods with the DM and ZINB-DPP models, and the five competitors, and computed their individual AUC and MCC. The average AUC over 50 simulated datasets under the same group number ( $K = 3$ ) and different sample sizes and effect sizes,  $(n, \sigma)$ , are displayed in Figure (3a) and (3c). It shows that all methods performed reasonably well for the data generated by the DM model when either the sample size or the effect size is fairly large, as shown in Figure (3a). However, for a small sample size ( $n = 24$ ) and a small effect size ( $\sigma = 1$ ), the performance of `edgeR`, `DESeq2`, and `metagenomeSeq` significantly dropped. For the data generated by the ZINB model, the results show that the ZINB-DPP model always achieved the highest AUC values. Decreasing either the sample size or the effect size would lead to greater disparity between ZINB-DPP and

the others. Figure (3b) and (3d) show the comparison in terms of MCC. To make a fair comparison between the methods who output  $p$ -values and who output probability measures such as PPI, we picked only the top 50 significant features of each dataset from each method and computed their individual MCC. These two plots confirm the overall best performance of our proposed ZINB-DPP model. The ZINB-DPP model also shows very competitive performance on the synthetic data. The results of the average AUC and MCC are presented in Figure (4a) and (4b). Note that we generated the synthetic datasets from the a multinomial model whose parameters were estimated by using the skin/feces samples collected by Caporaso et al. (2011). Therefore, they ought to favor our DM model. However, the ZINB-DPP model, again, maintained the highest MCCs across all scenarios, and the DM model performed the second-best in general. Additionally, all methods showed great improvement when increasing the sample size or the effect size, which was expected. We only show the results from skin samples here and the plots of feces, which lead to the same findings, are shown in the supplement. Results from the ZINB model with alternative normalization methods are also included in the supplement.

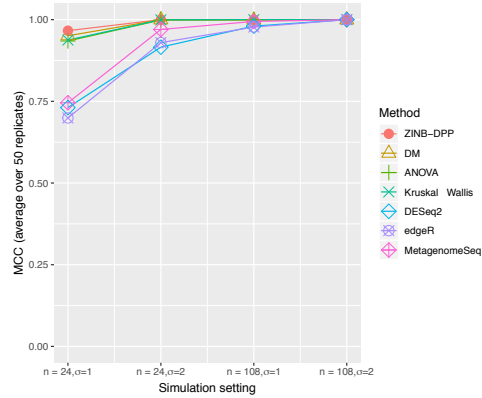
## 5 Real Data Analysis

### 5.1 Colorectal cancer study

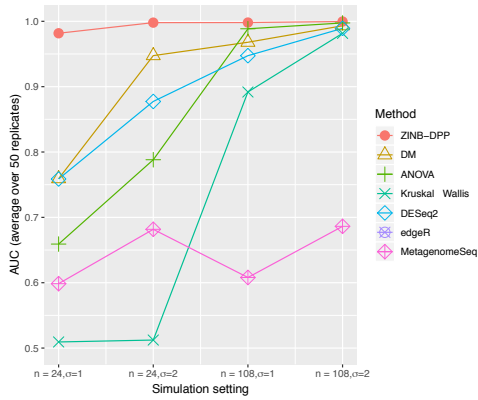
Colorectal cancer (CRC) is a disease originating from the epithelial cells lining the colon or rectum of the gastrointestinal tract. There have been an increasing number of studies revealing the association between CRC and the microbiome (Marchesi et al. 2011, Ahn et al. 2013, Sears & Garrett 2014). We applied our model to a colorectal cancer gut microbiome dataset published by Zeller et al. (2014). The cohort consists of 199 individuals from Europe and (133 patients with CRC or adenoma(s) as cases, and 66 healthy patients as controls). The disease status was determined by colonoscopy. The



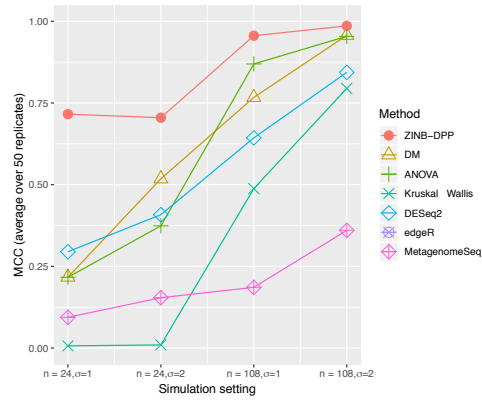
(a) DM simulation: AUC by different methods



(b) DM simulation: MCC by different methods



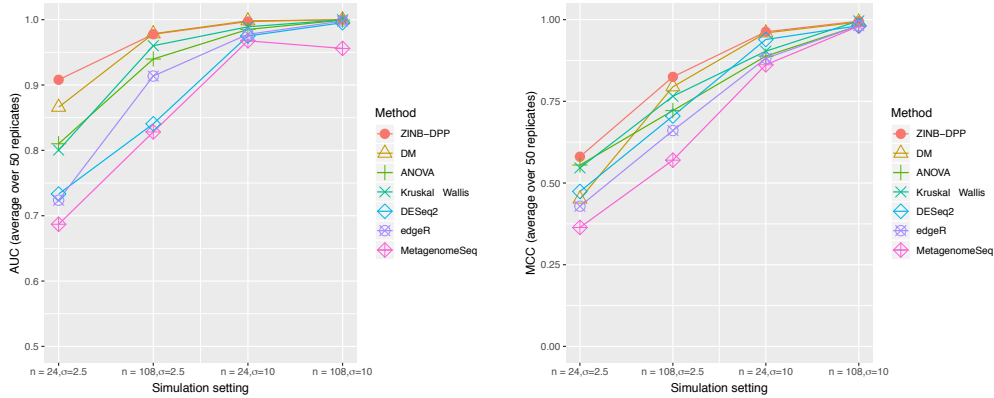
(c) ZINB simulation: AUC by different methods



(d) ZINB simulation: MCC by different methods

**Figure 3:** Simulation study: The average AUC and MCC achieved by the proposed framework with the DM model and ZINB model, and the five competitors: ANOVA, Kruskal-Wallis, edgeR, DESeq2, and metagenomeSeq. (a) and (b) are plotted from the simulated data generated by the DM model. (c) and (d) are plotted from the simulated data generated by the ZINB model.

original metagenomic sequence data were available from the European Nucleotide Archive database (accession number ERP005534). We used MetaPhlan2 (Truong et al. 2015) and curatedMetagenomicData (Pasolli et al. 2017) to obtain the taxonomic abundance table. In total, there were 3,940 taxa detected from the fecal samples of the patients.



(a) AUC by different methods for synthetic dataset (b) MCC by different methods for synthetic dataset

**Figure 4:** Simulation study: The average AUC and MCC achieved by the proposed framework with DM model and ZINB model, and the five competitors: ANOVA, Kruskal-Wallis, edgeR, DESeq2, and metagenomeSeq. (a) and (b) are plotted from the synthetic data generated by the multinational model of skin samples. (c) and (d) are plotted from the synthetic data generated by the multinational model of feces samples.

### 5.1.1 Quality control

Before analyzing a given microbiome count dataset, we first implemented a simple quality control step. It ensures that the dataset is of the best quality to perform the subsequent modeling. This step includes: 1) examining the total number of reads sequenced, and 2) verifying the richness of taxa discovered. First, if the total number of reads for a sample falls above or below specific values (shown below), then this may indicate poor sequence quality owing to duplicate reads or limited sampling bias. Specifically, let  $y_i = \sum_{j=1}^p y_{ij}$  denote the total number of reads observed in sample  $i$ . A sample  $i$  will be removed if its total reads  $y_i < Q1 - 3(Q3 - Q1)$  or  $> Q3 + 3(Q3 - Q1)$ , where  $Q1$  and  $Q3$  are the lower and upper quartiles (i.e. 25% and 75% percentiles) of the total reads of all the samples (i.e.  $\{y_1, \dots, y_n\}$ ). Note that in the context of box-and-whisker plotting, a data point is defined as an extreme outlier if it stands outside these two limits. Second, in ecology, investigators find that the number of species increases as sampling effort increases. This species-

abundance distribution can be depicted by *the collector’s curve*, which is monotonically increasing and negatively accelerated. Hence, we assumed that the logarithmic count of taxa discovered in one sample has a linear relationship with the total reads observed in the same sample. As suggested by Hair et al. (2006), we fitted the regression model to compute the Cook’s distance for each sample, and removed the samples with distances above  $4/(n-2)$  since they were considered as the influential data points for a least-squares regression analysis. Finally, a total of  $n = 182$  samples were left after the quality control step. Another common procedure in microbiome studies, as mentioned by Sohn et al. (2015) and Wadsworth et al. (2017), is to filter out the extremely low-abundant taxa. In this CRC study, due to the imbalanced sample size between the patient groups, we found several taxa have only one nonzero read for patients with adenoma (42 patients in this group). Hence, we grouped these patients with the healthy controls together to form a single group “non-CRC”. Furthermore, following the idea in Sohn et al. (2015), we dropped the taxa with less than 3 nonzero reads in at least one of the two patient groups.

### 5.1.2 Results

We applied the proposed ZINB model with DPP to detect the differentially abundant taxa. We chose weakly informative priors as hyperparameters as discussed in Section 4. Specifically, we set the shape parameters  $a_0 = a_1 = \dots = a_k = 2$  and the scale parameters  $b_0 = b_1 = \dots = b_k = 1$  for variance components  $\sigma_{0j}^2$  and  $\sigma_{kj}^2$ . Next, we let  $h_0 = h_1 = \dots = h_K = 10$ . Finally, we specified  $M = n/2$ ,  $c_s = 0$ ,  $\sigma_s = 1$ ,  $\tau_\eta = 1$ ,  $a_t = b_t = 1$ ,  $a_m = b_m = 1$ ,  $a_\phi = b_\phi = 0.001$  and  $a_\pi = b_\pi = 1$ . Results reported below were obtained by combining the outputs from 4 MCMC chains after ensuring convergence. We used 20,000 iterations with a burn-in of the first 10,000 iterations. The pairwise correlation coefficients of PPI range from 0.969 to 0.993, suggesting the MCMC chains

has good convergence. The PPIs reported by the ZINB model for all taxa are shown in Figure (5a), where the dashed line represents a stringent threshold that controls the Bayesian FDR at less than 0.1%. Twenty four differentially abundant taxa whose PPI passed the threshold are shown in Figure (5c), and they are ranked based on the order of estimated  $\log(\alpha_{1j}/\alpha_{0j})$ .

Our top findings of CRC-enriched taxa are consistent with the results reported in the original study (Zeller et al. 2014). The authors trained a classification model using a combination of marker species to predict the group label for a patient. Among 22 gut microbial species that were collectively associated with CRC, they pointed out 4 species, including two subspecies from *Fusobacterium nucleatum*, *Peptostreptococcus stomatis* and *Porphyromonas asaccharolytica*, that were the most discriminative features in their ensemble classifier. These taxa were also the top differentially abundant species reported by our model. Moreover, many studies have verified the overabundance of *Fusobacterium nucleatum* (*Fn*) in CRC tumor versus normal control tissue and biologically validated its roles in tumorigenesis. Castellarin et al. (2012) showed, through an association study, that *Fn* may contribute to CRC development by invading colonic mucosa, which further induces local inflammation and an increasing expression of cytokines. Two other studies provided more convincing evidence that *Fn* infection directly contributes to colorectal carcinogenesis (Kostic et al. 2013, Rubinstein et al. 2013). They reported that *Fn* invasion would replenish tumor-infiltrating immune cells and generate an tumorigenic microenvironment that encourages colorectal neoplasia. Our model not only selected the phylogenetic tree of *Fn* from species level to phylum level (Figure (6a)), it also detected a branch of gram-negative bacteria, from *Campylobacter* to *Epsilonproteobacteria*. These findings support the conclusion from a previous CRC study by Warren et al. (2013), where they observed significant co-occurrence within individual tumors of *Fusobacterium* and *Campylobacter* species. However, the possibility that this polymicrobial signature

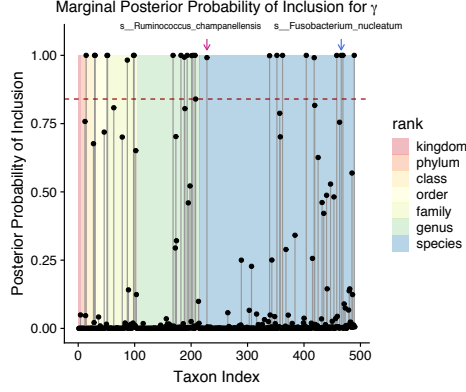
may have an etiological role in cinogenesis remains an open question that requires further study. As for other CRC-enriched species, a recent study has independently reported that the abundance of *Peptostreptococcus anaerobius* is elevated in patients with colorectal cancer (Tsoi et al. 2017). Moreover, *Peptostreptococcus stomatis* and *Parvimonas micra* were found to be enriched in a CRC subtype by Purcell et al. (2017). Besides the discovery of CRC-enriched taxa, our model also reported several non-CRC enriched taxa. *Ruminococcus champanellensis*, a strictly anaerobic bacteria, was a newly found species and less studied. However, its genus *Ruminococcus* is if often found to be decreased in colorectal cancer (Brennan & Garrett 2016). Similarly, *Eubacteriaceae* was found to be underrepresented in CRC tissue Marchesi et al. (2011). In all, among 10 differentially abundant species identified by our model, 7 of them were found to have solid biological evidences.

## 5.2 Schizophrenia study

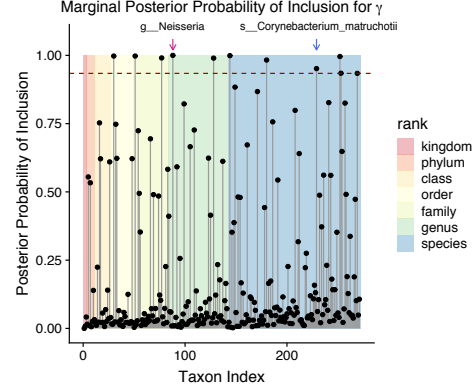
Schizophrenia is a neuropsychiatric disorder whose typical symptoms include hallucinations, delusions, social withdrawal, etc. It has recently been established that the gut microbiota plays a contributory role in psychiatric symptomatology (Fond et al. 2015), and is involved in diseases related to neurodevelopment and the programming of appropriate stress responses (Rea et al. 2016). We analyzed the metagenome-sequenced oropharynx samples of 16 schizophrenia patients and 16 controls studied by Castro-Nallar et al. (2015). We used the same bioinformatics software (MetaPhlAn2 and curatedMetagenomicData) and obtained taxonomic abundance matrix. We performed the quality control steps as implemented in Section 5.1 and removed 5 potential outlier samples. Meanwhile, since the sample size was relatively small compared to the previous study, we only excluded taxa with less than 2 nonzero reads in at least one of the two patient groups.

We fitted this dataset using the ZINB model with the DPP prior. We kept the de-

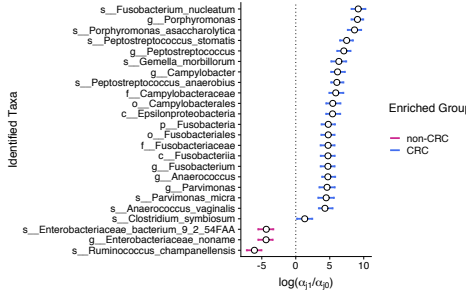




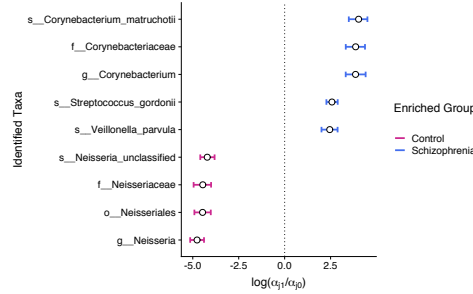
(a)  $\gamma$  PPI for the CRC study



(b)  $\gamma$  PPI for the schizophrenia study



(c) 95% credible intervals for  $\log(\alpha_{j1}/\alpha_{j0})$  of taxa detected in in CRC study



(d) 95% credible intervals for  $\log(\alpha_{j1}/\alpha_{j0})$  of taxa detected in the schizophrenia study

**Figure 5:** Case study: plots of  $\gamma$  PPI and 95% credible interval for two case studies. The horizontal dashed line in the PPI plot represents the threshold controlling the Bayesian false discovery rate (0.001 for CRC study; 0.01 for schizophrenia study). All taxa whose PPI pass the threshold are included in (c) and (d), where each horizontal bar is the 95% credible interval for  $\log(\alpha_{j1}/\alpha_{j0})$  of the corresponding discriminating taxon  $j$ .

fault prior specification described in Section 4.1. Four independent chains were run with randomly initialized starting points. After burning in the first half of 20,000 iterations for each chain, we calculated pairwise correlation coefficients of PPIs (ranging from 0.978 to 0.987) which indicated that the MCMC chains were convergent. The identified differentially abundant taxa and their enrichment directions are presented in Figure (5b) and (5d). In particular, our model selected four taxa all under the order level for *Neisseriales*

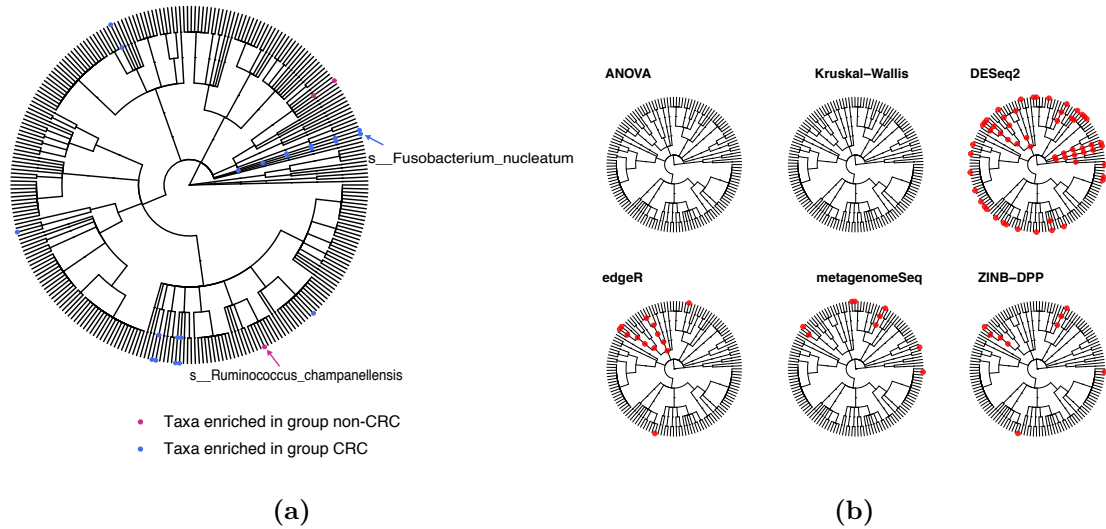


**Figure 6:** Real Data Analysis: cladograms of the identified discriminating taxa (shown in dots) in colorectal cancer study (a) and schizophrenia study (b). Each arrow in (a), (b) points out the taxon with largest absolute value of  $\log(\alpha_{1j}/\alpha_{0j})$  in one patient group as shown in Figure 5c and 5d.

(Figure 6b), and they were concluded to be the key members of the healthy oropharynx microbiome. Notably, 3 of them were also reported with the findings in the original paper. A recent study of attention-deficit/hyperactivity disorder (ADHA) showed that patients with ADHD had elevated levels of *Neisseriaceae* and *Neisseria spec* (Prehn-Kristensen et al. 2018). ADHD is a psychiatric disorder characterized by hyperactivity, impulsivity and attention problems. Interestingly, Hamshere et al. (2013) identified significant shared genetic susceptibility between childhood ADHD and schizophrenia. On the other hand, the top three case-enriched taxa all belonged to family *Corynebacteriaceae*. A relevant study by Strati et al. (2017) claimed the abundance of *Corynebacterium* was significantly increased for a cohort with autism spectrum disorder (a neurodevelopmental disorder). Bavaro et al. (2011) also claimed that a specific species from *Corynebacterium* was associated with the human neural protein network. All the aforementioned studies suggest a causal effect of *Corynebacterium* in mental disorders. Furthermore, altered levels of *Veillonellaceae* were observed between healthy people and patients in various studies of

nervous system disorders, such as autism, gastrointestinal disturbances and first episodes of psychosis (Kelly et al. 2017, Schwarz et al. 2018). Meanwhile, our model selected *Streptococcus gordonii* as a potential contributing factor to schizophrenia development. This specific species has not been widely investigated in psychiatric studies, and the adjusted  $p$ -value from the KruskalWallis test is above a significance level of 0.01. However, the small sample size ( $n = 27$ ), along with the presence of too many zeros (10 out of 27), undermines the reliability of the test results. As suggested by our model, biological validations would be a promising next step for better understanding the schizophrenia pathogenesis.

## 6 Conclusion

In this paper, we have proposed a Bayesian hierarchical framework for analyzing microbiome count data. Our bi-level framework offers flexibility to special normalization models and differential abundance analysis models, in distinct levels. Under this framework, we developed a Bayesian hierarchical model with the stochastic prior. We showed that this prior can reduce estimation bias and improved the posterior inferences of the other parameters of interests. Notably, our application of the Dirichlet process prior is not restricted to the microbiome data analysis, and it is generally applicable to other types of heterogeneous sequence data (Li et al. 2017). Moreover, our model can jointly analyze multiple microbes at different taxonomic levels while offering well-controlled Bayesian false discovery rates. In addition, our model is applicable for studies with more than 2 disease outcomes, such as multiple patient subtypes. Additionally, our model can support the detection of discriminating taxa among all patient subgroups or between any pair of them. The MCMC algorithm is implemented using the R package `Rcpp` to improve computational efficiency. These codes were used in all simulation and real data analyses.

They are available upon request from the corresponding authors.

As a summary of model performance, the ZINB-DPP model shows its promises. It consistently outperforms commonly used methods in model-based simulations, synthetic data simulations and two real data analyses. Specifically, it placed in the top 2 for simulated and synthetic data. It becomes more competitive as either the sample size or the effect size decreases. In two case studies, our results were consistent with the original studies, and our novel findings also provide promising guidance for further biological mechanism investigation. For researchers interested in more performance details, we evaluated other competing methods on the same datasets (CRC study and schizophrenia study) and present the results in the supplementary materials. Specifically, we noticed that the sparsity observed in microbiome data could impair the statistical power of ANOVA, especially when the sample size is small. Meanwhile, `edgeR` and `DESeq2` tend to have a higher false positive rate, whereas `metagenomeSeq` produces relatively conservative results compared to our model. These findings are consistent with (Weiss et al. 2017) and are helpful to future microbiome data analysis.

Our model framework can be naturally extended to other analysis scenarios. For example, the inferred latent abundance can be treated as within a sample normalized distribution. It is thus applicable to longitudinal analysis, which can capture the dynamic structure in microbiome studies; or to differential network analysis, which can investigate the complex interactions among microbial taxa. In all, our proposed Bayesian framework is extensible for multiple types of microbiome data analysis, and the implemented Bayesian model is useful for more powerful microbiome differential abundance analysis. We hope that all these contributions can be utilized to advance metagenomic data analysis.

## References

- Ahn, J., Sinha, R., Pei, Z., Dominianni, C., Wu, J., Shi, J., Goedert, J. J., Hayes, R. B. & Yang, L. (2013), ‘Human gut microbiome and risk for colorectal cancer’, *Journal of the National Cancer Institute* **105**(24), 1907–1911.
- Airoldi, E. M. & Bischof, J. M. (2016), ‘Improving and evaluating topic models and other models of text’, *Journal of the American Statistical Association* **111**(516), 1381–1403.
- Anders, S. & Huber, W. (2010), ‘Differential expression analysis for sequence count data’, *Genome Biology* **11**(10), R106.
- Ansorge, W. J. (2009), ‘Next-generation DNA sequencing techniques’, *New Biotechnology* **25**(4), 195–203.
- Bäckhed, F., Ley, R. E., Sonnenburg, J. L., Peterson, D. A. & Gordon, J. I. (2005), ‘Host-bacterial mutualism in the human intestine’, *Science* **307**(5717), 1915–1920.
- Banerjee, S., Carlin, B. P. & Gelfand, A. E. (2014), *Hierarchical modeling and analysis for spatial data*, CRC Press.
- Bavaro, S. L., Calabrò, M. & Kanduc, D. (2011), ‘Pentapeptide sharing between *Corynebacterium* diphtheria toxin and the human neural protein network’, *Immunopharmacology and Immunotoxicology* **33**(2), 360–372.
- Benjamini, Y. & Hochberg, Y. (1995), ‘Controlling the false discovery rate: a practical and powerful approach to multiple testing’, *Journal of the Royal Statistical Society. Series B* pp. 289–300.
- Brennan, C. A. & Garrett, W. S. (2016), ‘Gut microbiota, inflammation, and colorectal cancer’, *Annual Review of Microbiology* **70**, 395–411.

- Brown, C. T., Davis-Richardson, A. G., Giongo, A., Gano, K. A., Crabb, D. B., Mukherjee, N., Casella, G., Drew, J. C., Ilonen, J., Knip, M. et al. (2011), ‘Gut microbiome metagenomics analysis suggests a functional model for the development of autoimmunity for type 1 diabetes’, *PloS One* **6**(10), e25792.
- Brown, P. J., Vannucci, M. & Fearn, T. (1998), ‘Multivariate Bayesian variable selection and prediction’, *Journal of the Royal Statistical Society: Series B (Statistical Methodology)* **60**(3), 627–641.
- Bullard, J. H., Purdom, E., Hansen, K. D. & Dudoit, S. (2010), ‘Evaluation of statistical methods for normalization and differential expression in mRNA-Seq experiments’, *BMC Bioinformatics* **11**(1), 94.
- Cameron, A. C. & Trivedi, P. K. (2013), *Regression analysis of count data*, Vol. 53, Cambridge University Press.
- Caporaso, J. G., Lauber, C. L., Walters, W. A., Berg-Lyons, D., Lozupone, C. A., Turnbaugh, P. J., Fierer, N. & Knight, R. (2011), ‘Global patterns of 16S rRNA diversity at a depth of millions of sequences per sample’, *Proceedings of the National Academy of Sciences* **108**(Supplement 1), 4516–4522.
- Casella, G. & Berger, R. L. (2002), *Statistical Inference*, Vol. 2, Duxbury Pacific Grove, CA.
- Castellarin, M., Warren, R. L., Freeman, J. D., Dreolini, L., Krzywinski, M., Strauss, J., Barnes, R., Watson, P., Allen-Vercoe, E., Moore, R. A. et al. (2012), ‘*Fusobacterium nucleatum* infection is prevalent in human colorectal carcinoma’, *Genome Research* **22**(2), 299–306.
- Castro-Nallar, E., Bendall, M. L., Pérez-Losada, M., Sabuncyan, S., Severance, E. G., Dickerson, F. B., Schroeder, J. R., Yolken, R. H. & Crandall, K. A. (2015), ‘Compo-

- sition, taxonomy and functional diversity of the oropharynx microbiome in individuals with schizophrenia and controls’, *PeerJ* **3**, e1140.
- Chen, J. & Li, H. (2013), ‘Variable selection for sparse Dirichlet-multinomial regression with an application to microbiome data analysis’, *The Annals of Applied Statistics* **7**(1).
- Cheung, Y. B. (2002), ‘Zero-inflated models for regression analysis of count data: a study of growth and development’, *Statistics in Medicine* **21**(10), 1461–1469.
- Dillies, M.-A., Rau, A., Aubert, J., Hennequet-Antier, C., Jeanmougin, M., Servant, N., Keime, C., Marot, G., Castel, D., Estelle, J. et al. (2013), ‘A comprehensive evaluation of normalization methods for illumina high-throughput RNA sequencing data analysis’, *Briefings in Bioinformatics* **14**(6), 671–683.
- Fang, R., Wagner, B., Harris, J. & Fillon, S. (2016), ‘Zero-inflated negative binomial mixed model: an application to two microbial organisms important in oesophagitis’, *Epidemiology & Infection* **144**(11), 2447–2455.
- Fond, G., Boukouaci, W., Chevalier, G., Regnault, A., Eberl, G., Hamdani, N., Dickerson, F., Macgregor, A., Boyer, L., Dargel, A. et al. (2015), ‘The psychomicrobiotic: Targeting microbiota in major psychiatric disorders: A systematic review’, *Pathologie Biologie* **63**(1), 35–42.
- George, E. I. & McCulloch, R. E. (1997), ‘Approaches for Bayesian variable selection’, *Statistica Sinica* pp. 339–373.
- Hair, J. F., Black, W. C., Babin, B. J., Anderson, R. E., Tatham, R. L. et al. (2006), ‘Multivariate data analysis (vol. 6)’.
- Hamshere, M. L., Stergiakouli, E., Langley, K., Martin, J., Holmans, P., Kent, L., Owen, M. J., Gill, M., Thapar, A., O’donovan, M. et al. (2013), ‘Shared polygenic contribution

- between childhood attention-deficit hyperactivity disorder and adult schizophrenia’, *The British Journal of Psychiatry* **203**(2), 107–111.
- Holmes, I., Harris, K. & Quince, C. (2012), ‘Dirichlet multinomial mixtures: generative models for microbial metagenomics’, *PloS One* **7**(2), e30126.
- Honda, K. & Littman, D. R. (2012), ‘The microbiome in infectious disease and inflammation’, *Annual Review of Immunology* **30**, 759–795.
- Kelly, J. R., Minuto, C., Cryan, J. F., Clarke, G. & Dinan, T. G. (2017), ‘Cross talk: the microbiota and neurodevelopmental disorders’, *Frontiers in Neuroscience* **11**, 490.
- Kostic, A. D., Chun, E., Robertson, L., Glickman, J. N., Gallini, C. A., Michaud, M., Clancy, T. E., Chung, D. C., Lochhead, P., Hold, G. L. et al. (2013), ‘*Fusobacterium nucleatum* potentiates intestinal tumorigenesis and modulates the tumor-immune microenvironment’, *Cell Host & Microbe* **14**(2), 207–215.
- Kyung, M., Gill, J. & Casella, G. (2011), ‘Sampling schemes for generalized linear Dirichlet process random effects models’, *Statistical Methods & Applications* **20**(3), 259–290.
- La Rosa, P. S., Brooks, J. P., Deych, E., Boone, E. L., Edwards, D. J., Wang, Q., Sodergren, E., Weinstock, G. & Shannon, W. D. (2012), ‘Hypothesis testing and power calculations for taxonomic-based human microbiome data’, *PloS One* **7**(12), e52078.
- La Rosa, P. S., Zhou, Y., Sodergren, E., Weinstock, G. & Shannon, W. D. (2015), Hypothesis testing of metagenomic data, in ‘Metagenomics for Microbiology’, Elsevier, pp. 81–96.
- Lee, J. & Sison-Mangus, M. (2018), ‘A Bayesian semiparametric regression model for joint analysis of microbiome data’, *Frontiers in Microbiology* **9**, 522.



- Li, H. (2015), ‘Microbiome, metagenomics, and high-dimensional compositional data analysis’, *Annual Review of Statistics and Its Application* **2**, 73–94.
- Li, J., Witten, D. M., Johnstone, I. M. & Tibshirani, R. (2012), ‘Normalization, testing, and false discovery rate estimation for RNA-sequencing data’, *Biostatistics* **13**(3), 523–538.
- Li, Q., Cassese, A., Guindani, M. & Vannucci, M. (2018), ‘Bayesian negative binomial mixture regression models for the analysis of sequence count and methylation data’, *Biometrics* .
- Li, Q., Guindani, M., Reich, B. J., Bondell, H. D. & Vannucci, M. (2017), ‘A Bayesian mixture model for clustering and selection of feature occurrence rates under mean constraints’, *Statistical Analysis and Data Mining: The ASA Data Science Journal* **10**(6), 393–409.
- Love, M. I., Huber, W. & Anders, S. (2014), ‘Moderated estimation of fold change and dispersion for RNA-seq data with DESeq2’, *Genome Biology* **15**(12), 550.
- Mandal, S., Van Treuren, W., White, R. A., Eggesbø, M., Knight, R. & Peddada, S. D. (2015), ‘Analysis of composition of microbiomes: a novel method for studying microbial composition’, *Microbial Ecology in Health and Disease* **26**(1), 27663.
- Marchesi, J. R., Dutilh, B. E., Hall, N., Peters, W. H., Roelofs, R., Boleij, A. & Tjalsma, H. (2011), ‘Towards the human colorectal cancer microbiome’, *PloS One* **6**(5), e20447.
- Matthews, B. W. (1975), ‘Comparison of the predicted and observed secondary structure of T4 phage lysozyme’, *Biochimica et Biophysica Acta (BBA)-Protein Structure* **405**(2), 442–451.

- McMurdie, P. J. & Holmes, S. (2014), ‘Waste not, want not: why rarefying microbiome data is inadmissible’, *PLoS Computational Biology* **10**(4), e1003531.
- Metzker, M. L. (2010), ‘Sequencing technology the next generation’, *Nature Reviews Genetics* **11**(1), 31.
- Mosimann, J. E. (1962), ‘On the compound multinomial distribution, the multivariate  $\beta$ -distribution, and correlations among proportions’, *Biometrika* **49**(1/2), 65–82.
- Newton, M. A., Noueir, A., Sarkar, D. & Ahlquist, P. (2004), ‘Detecting differential gene expression with a semiparametric hierarchical mixture method’, *Biostatistics* **5**(2), 155–176.
- Pasolli, E., Schiffer, L., Manghi, P., Renson, A., Obenchain, V., Truong, D. T., Beghini, F., Malik, F., Ramos, M., Dowd, J. B. et al. (2017), ‘Accessible, curated metagenomic data through ExperimentHub’, *Nature Methods* **14**(11), 1023.
- Paulson, J. N., Stine, O. C., Bravo, H. C. & Pop, M. (2013), ‘Differential abundance analysis for microbial marker-gene surveys’, *Nature Methods* **10**(12), 1200.
- Peng, X., Li, G. & Liu, Z. (2016), ‘Zero-inflated beta regression for differential abundance analysis with metagenomics data’, *Journal of Computational Biology* **23**(2), 102–110.
- Prehn-Kristensen, A., Zimmermann, A., Tittmann, L., Lieb, W., Schreiber, S., Baving, L. & Fischer, A. (2018), ‘Reduced microbiome alpha diversity in young patients with ADHD’, *PloS One* **13**(7), e0200728.
- Purcell, R. V., Visnovska, M., Biggs, P. J., Schmeier, S. & Frizelle, F. A. (2017), ‘Distinct gut microbiome patterns associate with consensus molecular subtypes of colorectal cancer’, *Scientific Reports* **7**(1), 11590.

- Rea, K., Dinan, T. G. & Cryan, J. F. (2016), ‘The microbiome: a key regulator of stress and neuroinflammation’, *Neurobiology of Stress* **4**, 23–33.
- Robinson, M. D., McCarthy, D. J. & Smyth, G. K. (2010), ‘edgeR: a Bioconductor package for differential expression analysis of digital gene expression data’, *Bioinformatics* **26**(1), 139–140.
- Robinson, M. D. & Oshlack, A. (2010), ‘A scaling normalization method for differential expression analysis of RNA-seq data’, *Genome Biology* **11**(3), R25.
- Rubinstein, M. R., Wang, X., Liu, W., Hao, Y., Cai, G. & Han, Y. W. (2013), ‘*Fusobacterium nucleatum* promotes colorectal carcinogenesis by modulating E-cadherin  $\beta$ -catenin signaling via its FadA adhesin’, *Cell Host & Microbe* **14**(2), 195–206.
- Schwarz, E., Maukonen, J., Hyytiäinen, T., Kieseppä, T., Orešič, M., Sabunciyan, S., Mantere, O., Saarela, M., Yolken, R. & Suvisaari, J. (2018), ‘Analysis of microbiota in first episode psychosis identifies preliminary associations with symptom severity and treatment response’, *Schizophrenia Research* **192**, 398–403.
- Sears, C. L. & Garrett, W. S. (2014), ‘Microbes, microbiota, and colon cancer’, *Cell Host & Microbe* **15**(3), 317–328.
- Sohn, M. B., Du, R. & An, L. (2015), ‘A robust approach for identifying differentially abundant features in metagenomic samples’, *Bioinformatics* **31**(14), 2269–2275.
- Stingo, F. C., Guindani, M., Vannucci, M. & Calhoun, V. D. (2013), ‘An integrative Bayesian modeling approach to imaging genetics’, *Journal of the American Statistical Association* **108**(503), 876–891.
- Strati, F., Cavalieri, D., Albanese, D., De Felice, C., Donati, C., Hayek, J., Jousson, O.,

- Leoncini, S., Renzi, D., Calabrò, A. et al. (2017), ‘New evidences on the altered gut microbiota in autism spectrum disorders’, *Microbiome* **5**(1), 24.
- Taddy, M. A. & Kottas, A. (2012), ‘Mixture modeling for Marked Poisson processes’, *Bayesian Analysis* **7**(2), 335–362.
- Tadesse, M. G., Sha, N. & Vannucci, M. (2005), ‘Bayesian variable selection in clustering high-dimensional data’, *Journal of the American Statistical Association* **100**(470), 602–617.
- Trippa, L. & Parmigiani, G. (2011), ‘False discovery rates in somatic mutation studies of cancer’, *The Annals of Applied Statistics* pp. 1360–1378.
- Truong, D. T., Franzosa, E. A., Tickle, T. L., Scholz, M., Weingart, G., Pasolli, E., Tett, A., Huttenhower, C. & Segata, N. (2015), ‘MetaPhlAn2 for enhanced metagenomic taxonomic profiling’, *Nature Methods* **12**(10), 902.
- Tsoi, H., Chu, E. S., Zhang, X., Sheng, J., Nakatsu, G., Ng, S. C., Chan, A. W., Chan, F. K., Sung, J. J. & Yu, J. (2017), ‘*Peptostreptococcus anaerobius* induces intracellular cholesterol biosynthesis in colon cells to induce proliferation and causes dysplasia in mice’, *Gastroenterology* **152**(6), 1419–1433.
- Wadsworth, W. D., Argiento, R., Guindani, M., Galloway-Pena, J., Shelburne, S. A. & Vannucci, M. (2017), ‘An integrative Bayesian Dirichlet-multinomial regression model for the analysis of taxonomic abundances in microbiome data’, *BMC Bioinformatics* **18**(1), 94.
- Warren, R. L., Freeman, D. J., Pleasance, S., Watson, P., Moore, R. A., Cochrane, K., Allen-Vercoe, E. & Holt, R. A. (2013), ‘Co-occurrence of anaerobic bacteria in colorectal carcinomas’, *Microbiome* **1**(1), 16.

- Weiss, S., Xu, Z. Z., Peddada, S., Amir, A., Bittinger, K., Gonzalez, A., Lozupone, C., Zaneveld, J. R., Vázquez-Baeza, Y., Birmingham, A. et al. (2017), ‘Normalization and microbial differential abundance strategies depend upon data characteristics’, *Microbiome* **5**(1), 27.
- Witten, D. M. (2011), ‘Classification and clustering of sequencing data using a Poisson model’, *The Annals of Applied Statistics* pp. 2493–2518.
- Xia, Y. & Sun, J. (2017), ‘Hypothesis testing and statistical analysis of microbiome’, *Genes & Diseases* **4**(3), 138–148.
- Xu, L., Paterson, A. D., Turpin, W. & Xu, W. (2015), ‘Assessment and selection of competing models for zero-inflated microbiome data’, *PloS One* **10**(7), e0129606.
- Zeller, G., Tap, J., Voigt, A. Y., Sunagawa, S., Kultima, J. R., Costea, P. I., Amiot, A., Böhm, J., Brunetti, F., Habermann, N. et al. (2014), ‘Potential of fecal microbiota for early-stage detection of colorectal cancer’, *Molecular Systems Biology* **10**(11), 766.
- Zhang, X., Mallick, H., Tang, Z., Zhang, L., Cui, X., Benson, A. K. & Yi, N. (2017), ‘Negative binomial mixed models for analyzing microbiome count data’, *BMC Bioinformatics* **18**(1), 4.
- Zhang, X., Mallick, H. & Yi, N. (2016), ‘Zero-inflated negative binomial regression for differential abundance testing in microbiome studies’, *Journal of Bioinformatics and Genomics* (2 (2)).

# Bayesian Modeling of Microbiome Data for Differential Abundance Analysis Supplementary Material

Qiwei Li <sup>\*</sup> <sup>1</sup>, Shuang Jiang<sup>\*</sup> <sup>2, 4</sup>, Andrew Y. Koh <sup>3</sup>, Guanghua Xiao<sup>†4</sup> and  
Xiaowei Zhan <sup>†4</sup>

<sup>1</sup>Center for Depression Research and Clinical Care, University of Texas  
Southwestern Medical Center

<sup>2</sup>Department of Statistical Science, Southern Methodist University

<sup>3</sup>Departments of Pediatrics and Microbiology, University of Texas  
Southwestern Medical Center

<sup>4</sup>Quantitative Biomedical Research Center, Department of Population  
and Data Sciences, University of Texas Southwestern Medical Center

---

<sup>\*</sup>These authors contributed equally to this work.

<sup>†</sup>To whom correspondence should be addressed.

# 1 Results of Simulation Study

We performed a comprehensive simulation study for model comparison. Tables (1) to (3) present the full results of different models on both simulated and synthetic datasets. In particular, Tables (1) and (2) evaluate the model performance with respect to area under the curve (AUC) and Matthews correlation coefficient (MCC) on data generated from DM and ZINB model. Different methods were compared under  $2^4 = 16$  scenarios, including the two bottom-level kernels ( $\{\text{DM}, \text{ZINB}\}$ ), the two choices of the sample size ( $n \in \{24, 108\}$ ), the number of groups ( $K \in \{2, 3\}$ ) and the log effect size ( $\sigma \in \{1, 2\}$ ). Table (3) compares the AUC and MCC for all methods implemented on the synthetic data. There are  $2^3 = 8$  settings: the two types of samples ( $\{\text{Skin}, \text{Feces}\}$ ), the two choices of the sample size ( $n \in \{24, 108\}$ ) and the log effect size ( $\sigma \in \{1, 2\}$ ). To make a fair comparison between the methods who output  $p$ -values and who output probability measures such as PPI, we picked only the top 50 significant features of each dataset from each method and computed their individual MCC. Notice that ZINB-RLE and `edgeR` failed to produce any results on data generated by the ZINB model, as shown in Table (1) and (2). Both methods estimate the size factor using RLE, and a large number of random zeros is likely to make the geometric means of a few features inadmissible. Hence, these two methods failed due to their invalid size factor estimation.

## 2 Sensitivity Analysis

In this section, we examined the model sensitivity with respect to the choice of hyperparameters  $b_0, \dots, b_K$  and  $h_0, \dots, h_K$ . The results in Table (4) show that our approach is insensitive to these hyperparameter.

The choice of  $b_k$  and  $h_k$  for  $k = 0, \dots, K$  are related to the variance terms in the Gaussian mixture model. Large values of  $h_k$  would achieve a noninformative prior on

$\mu_{kj}$ 's. On the other hand, as we specified  $\text{IG}(a_k, b_k)$  prior for  $\sigma_{kj}^2$  and set  $a_k = 2$  for all  $k = 0, \dots, K$ , the resulted variance of inverse gamma distribution does not exist. We considered a range of  $(b_k, h_k)$  settings as  $b_k \in \{0.1, 1, 2, 10\}$  and  $h_k \in \{1, 10, 100\}$ . Then we applied the ZINB-DPP model with different combinations of  $(b_k, h_k)$  to datasets simulated from the ZINB model discussed in Section 4 in the main text. To fully assess the impact of hyperparameters under different scenarios, we considered  $K = 2, 3$  and  $n = 24, 108$  with a weakly discriminating signal  $\sigma = 1$ . We generated 50 independent datasets for each case and reported the averaged AUC (in Table (4)). Clearly, the AUC stayed stable for different choices of  $(b_k, h_k)$ . Therefore, we propose to set  $b_k = 1$  and  $h_k$  to be any value ranging from 10 to 100 for  $k = 1, \dots, K$ .

### 3 Real Data Analysis: Comparison with Alternative Approaches

Similarly to the simulation study conducted in the paper, we compared results given by our proposed model on the case study data with those from alternative approaches, including ANOVA, KruskalWallis test, DESeq2, edgeR and metagenomeSeq.

#### 3.1 Colorectal cancer study

We adopted a 0.1% significance level threshold on the Benjamini-Hochberg adjusted p-values provided by the alternative methods. The choice of 0.1% was set to be consistent with the Bayesian false discovery rate (FDR) of the ZINB-DPP model. Figure (1) compares all the results. First, ANOVA lacked statistical power when the data contain too many zeros, and it failed to identify any discriminating taxa in this case. The KruskalWallis test identified 17 discriminating taxa, 15 of which were also reported by ZINB-DPP model. Although KruskalWallis selected the branch of species *Fusobacterium nucleatum*



as we did, it failed to detect the co-occurrence between *Fusobacterium nucleatum* and *Campylobacter* by our model. Next, under a stringent significance level of 0.1%, DESeq2 and edgeR still led to the selection of 149 and 45 discriminating taxa, respectively. The large number of detections might suggest a high FDR. Further, edgeR failed to detect the genus to phylum levels of *Fusobacterium nucleatum* as most of other methods did. Lastly, we found that metagenomeSeq performed conservatively, as it only reported 7 discriminating taxa, 6 of which were consistent with the result by ZINB-DPP. Clearly, its result failed to reflect any phylogenetic tree structure.

### 3.2 Schizophrenia study

Under a 1% significance level threshold on the Benjamini-Hochberg adjusted p-values, we evaluated the performance of the alternative methods on the schizophrenia study. The results are shown in Figure (2). All the methods were challenged by the small sample size ( $n = 27$ ), along with the inflated amount of zeros. DESeq2 and edgeR led to the selection of 58 and 13 discriminating taxa, while the ANOVA and KruskalWallis tests failed to report any result. Out of the taxa selected by DESeq2 and edgeR, respectively, 9 and 5 were in the list of taxa found by our model (ZINB-DPP selected 9 under the Bayesian FDR of 1%). 4 out of the 8 taxa identified by edgeR but not our method were also selected by DESeq2. However, DESeq2 did not include the phylogenetic tree branch from *Corynebacterium matruchotii* to *Corynebacteriaceae*, which were reported by both metagenomeSeq and ZINB-DPP model. metagenomeSeq also identified 9 taxa under the significance level of 1%, 6 of which were consistent with the ZINB-DPP model. We noticed that metagenomeSeq only identified *Neisseria sp.* and *Neisseria* as in the phylogenetic tree branch, whereas all the remaining methods reached to the order level *Neisseriales*. Meanwhile, *Veillonella parvula* reported by ZINB-DPP, DESeq2 and edgeR was not identified by metagenomeSeq.

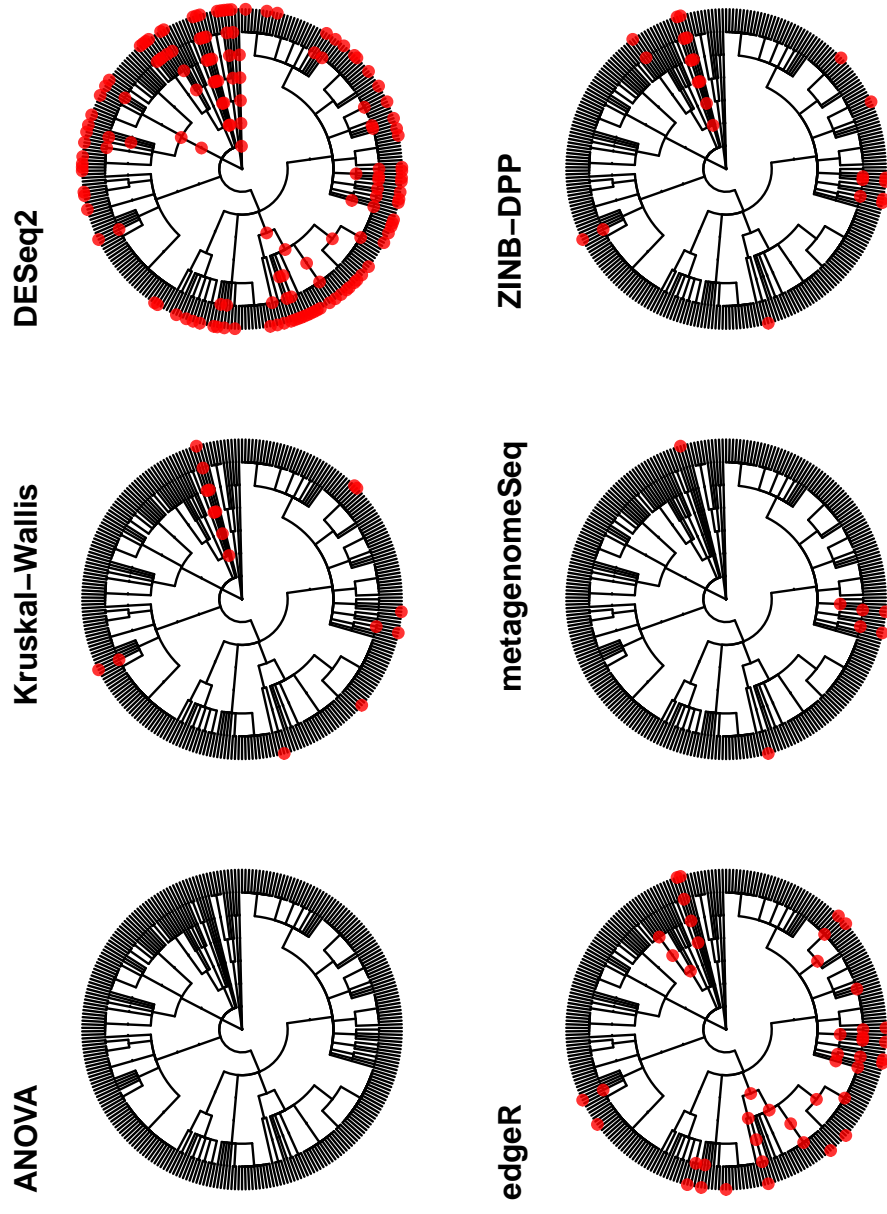


**Figure 1:** Colorectal cancer study: the discriminating taxa identified by different methods. The red dots in each of the first 5 cases represent the taxa with Benjamini-Hochberg adjusted  $p$ -values below the significance level of 0.1%. The red dots in the ZINB-DPP are taxa detected by controlling the Bayesian FDR to be less than 0.1%.

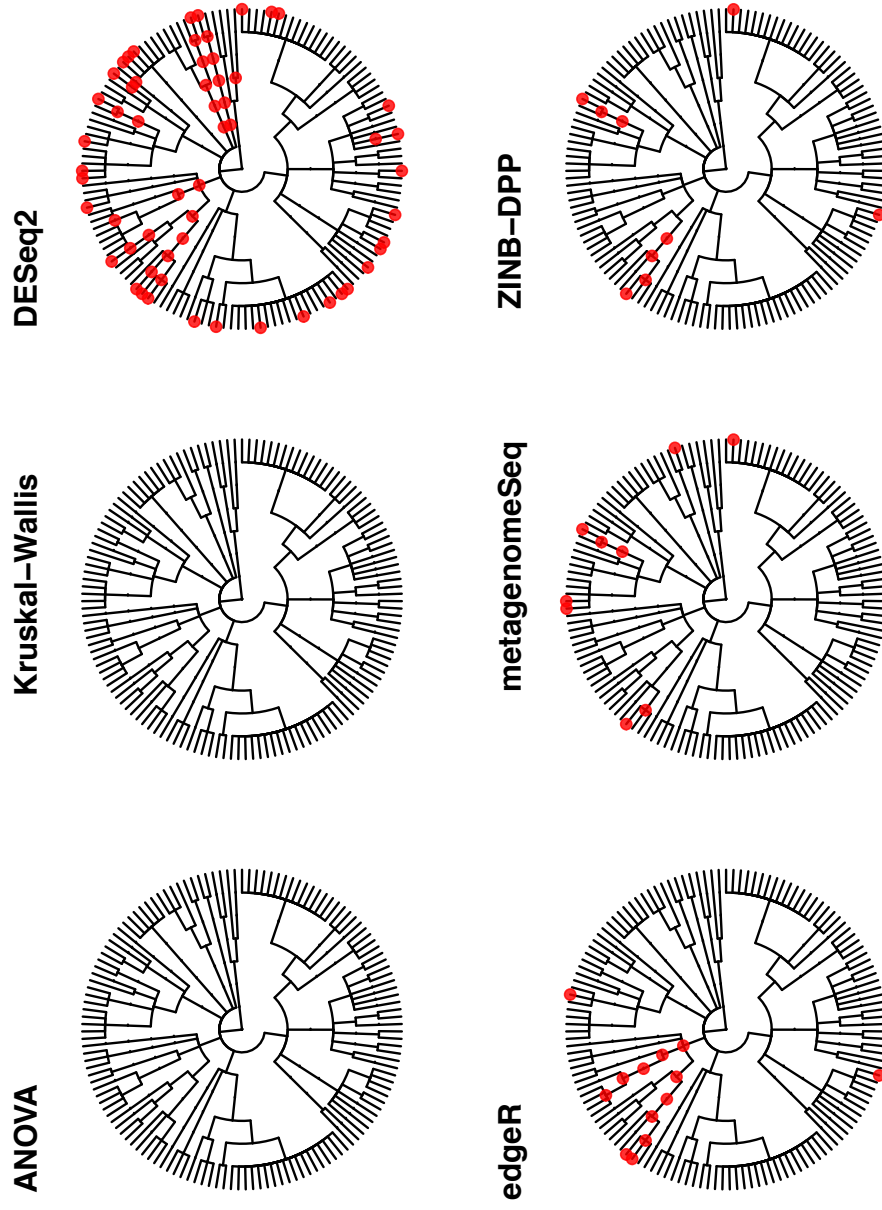


**Figure 2:** Schizophrenia study : the discriminating taxa identified by different methods. The red dots in each of the first 5 cases represent the taxa with Benjamini-Hochberg adjusted  $p$ -values below the significance level of 1%. The red dots in the ZINB-DPP are taxa detected by controlling the Bayesian FDR to be less than 1%.

Generative Model	Methods	Simulation Setting							
		$K = 2$				$K = 3$			
		$n = 24$		$n = 108$		$n = 24$		$n = 108$	
		$\sigma = 1$	$\sigma = 2$	$\sigma = 1$	$\sigma = 2$	$\sigma = 1$	$\sigma = 2$	$\sigma = 1$	$\sigma = 2$
DM	ZINB-DPP	<b>1.000</b> (0.0102)	<b>1.000</b> (0.0000)	<b>1.000</b> (0.0000)	<b>1.000</b> (0.0000)	<b>1.000</b> (0.0003)	<b>1.000</b> (0.0000)	<b>1.000</b> (0.0000)	<b>1.000</b> (0.0000)
	ZINB-TSS	0.977 (0.0111)	1.000 (0.0002)	1.000 (0.0002)	1.000 (0.0001)	0.999 (0.0006)	1.000 (0.0002)	1.000 (0.0001)	1.000 (0.0002)
	ZINB-Q75	0.977 (0.0112)	1.000 (0.0001)	1.000 (0.0001)	1.000 (0.0001)	0.999 (0.0005)	<b>1.000</b> (0.0000)	<b>1.000</b> (0.0000)	1.000 (0.0001)
	ZINB-RLE	0.978 (0.0100)	1.000 (0.0001)	1.000 (0.0001)	<b>1.000</b> (0.0000)	1.000 (0.0004)	<b>1.000</b> (0.0000)	1.000 (0.0001)	1.000 (0.0001)
	ZINB-TMM	0.978 (0.0105)	1.000 (0.0001)	1.000 (0.0001)	<b>1.000</b> (0.0000)	1.000 (0.0005)	<b>1.000</b> (0.0000)	1.000 (0.0001)	1.000 (0.0001)
	ZINB-CSS	0.976 (0.0115)	<b>1.000</b> (0.0000)	1.000 (0.0000)	1.000 (0.0001)	0.999 (0.0008)	<b>1.000</b> (0.0000)	1.000 (0.0001)	1.000 (0.0001)
	DM	0.972 (0.0111)	1.000 (0.0002)	1.000 (0.0002)	1.000 (0.0001)	0.999 (0.0006)	1.000 (0.0002)	1.000 (0.0001)	1.000 (0.0002)
	ANOVA	0.977 (0.0101)	1.000 (0.0003)	1.000 (0.0003)	1.000 (0.0004)	0.999 (0.0010)	1.000 (0.0004)	1.000 (0.0003)	1.000 (0.0004)
	KruskalWallis	0.978 (0.0102)	1.000 (0.0002)	1.000 (0.0003)	1.000 (0.0004)	0.999 (0.0008)	1.000 (0.0001)	1.000 (0.0003)	1.000 (0.0003)
	DeSeq2	0.981 (0.0094)	1.000 (0.0005)	1.000 (0.0004)	0.999 (0.0004)	0.961 (0.0154)	0.997 (0.0033)	0.999 (0.0008)	1.000 (0.0004)
	edgeR	0.969 (0.0130)	0.999 (0.0006)	1.000 (0.0005)	1.000 (0.0006)	0.945 (0.0237)	0.996 (0.0049)	0.999 (0.0007)	1.000 (0.0004)
	metagenomeSeq	0.957 (0.0146)	0.998 (0.0017)	0.895 (0.0239)	0.918 (0.0199)	0.972 (0.0122)	0.999 (0.0015)	0.992 (0.0043)	0.994 (0.0040)
ZINB	ZINB-DPP	<b>0.907</b> (0.0203)	<b>0.990</b> (0.0095)	<b>0.994</b> (0.0051)	<b>0.998</b> (0.0039)	<b>0.982</b> (0.0085)	0.998 (0.0072)	<b>0.998</b> (0.0026)	<b>1.000</b> (0.0003)
	ZINB-TSS	0.888 (0.0240)	0.988 (0.0097)	0.993 (0.0059)	0.997 (0.0047)	0.975 (0.0125)	<b>0.998</b> (0.0065)	0.997 (0.0044)	1.000 (0.0005)
	ZINB-Q75	0.888 (0.0225)	0.988 (0.0101)	0.991 (0.0070)	0.997 (0.0051)	0.975 (0.0106)	0.998 (0.0043)	0.997 (0.0043)	1.000 (0.0005)
	ZINB-RLE	NA (-)	NA (-)	NA (-)	NA (-)	NA (-)	NA (-)	NA (-)	NA (-)
	ZINB-TMM	0.887 (0.0247)	0.988 (0.0103)	0.992 (0.0064)	0.997 (0.0045)	0.974 (0.0116)	0.998 (0.0062)	0.997 (0.0040)	<b>1.000</b> (0.0003)
	ZINB-CSS	0.881 (0.0245)	0.988 (0.0094)	0.991 (0.0073)	0.997 (0.0049)	0.973 (0.0128)	0.998 (0.0046)	0.997 (0.0047)	<b>1.000</b> (0.0003)
	DM	0.659 (0.0378)	0.856 (0.0261)	0.929 (0.0173)	0.990 (0.0109)	0.759 (0.0499)	0.947 (0.0245)	0.968 (0.0175)	0.993 (0.0098)

Generative Model	Methods	Simulation Setting							
		$K = 2$				$K = 3$			
		$n = 24$		$n = 108$		$n = 24$		$n = 108$	
		$\sigma = 1$	$\sigma = 2$	$\sigma = 1$	$\sigma = 2$	$\sigma = 1$	$\sigma = 2$	$\sigma = 1$	$\sigma = 2$
ZINB	ANOVA	0.714 (0.0601)	0.908 (0.0333)	0.972 (0.0126)	0.995 (0.0052)	0.659 (0.0689)	0.788 (0.0608)	0.989 (0.0066)	0.997 (0.0031)
	KruskalWallis	0.547 (0.0528)	0.634 (0.0834)	0.824 (0.0331)	0.942 (0.0197)	0.509 (0.0211)	0.512 (0.0216)	0.892 (0.0299)	0.982 (0.0098)
	DeSeq2	0.761 (0.0369)	0.937 (0.0239)	0.969 (0.0151)	0.993 (0.0077)	0.759 (0.0429)	0.877 (0.0418)	0.947 (0.0255)	0.989 (0.0079)
	edgeR	NA (-)	NA (-)	NA (-)	NA (-)	NA (-)	NA (-)	NA (-)	NA (-)
	metagenomeSeq	0.609 (0.0410)	0.766 (0.0443)	0.750 (0.0401)	0.933 (0.0252)	0.599 (0.0555)	0.682 (0.0697)	0.608 (0.0493)	0.686 (0.0535)

**Table 1:** DM and ZINB simulation: area under the curve (AUC) given by all methods. In each cell, the top number is the averaged AUC over 50 independent datasets, and the bottom number in parentheses is the standard error. Result from the model that achieved best performance under the associated scenario (each column) is marked in bold.

Generative Model	Methods	Simulation Setting							
		$K = 2$				$K = 3$			
		$n = 24$		$n = 108$		$n = 24$		$n = 108$	
		$\sigma = 1$	$\sigma = 2$	$\sigma = 1$	$\sigma = 2$	$\sigma = 1$	$\sigma = 2$	$\sigma = 1$	$\sigma = 2$
DM	ZINB-DPP	<b>0.800</b> (0.0379)	0.997 (0.0074)	0.999 (0.0042)	1.000 (0.0000)	<b>0.966</b> (0.0180)	<b>1.000</b> (0.0000)	<b>1.000</b> (0.0000)	<b>1.000</b> (0.0000)
	ZINB-TSS	0.779 (0.0474)	0.996 (0.0082)	0.999 (0.0042)	1.000 (0.0030)	0.954 (0.0260)	<b>1.000</b> (0.0000)	1.000 (0.0030)	<b>1.000</b> (0.0000)
	ZINB-Q75	0.777 (0.0479)	0.996 (0.0085)	0.999 (0.0051)	0.998 (0.0058)	0.957 (0.0267)	1.000 (0.0000)	1.000 (0.0030)	1.000 (0.0030)
	ZINB-RLE	0.782 (0.0495)	0.995 (0.0091)	1.000 (0.0030)	1.000 (0.0000)	0.960 (0.0220)	1.000 (0.0000)	0.999 (0.0042)	1.000 (0.0030)
	ZINB-TMM	0.776 (0.0451)	0.995 (0.0091)	0.999 (0.0042)	0.999 (0.0042)	0.957 (0.0224)	<b>1.000</b> (0.0000)	1.000 (0.0030)	<b>1.000</b> (0.0000)
	ZINB-CSS	0.774 (0.0494)	0.995 (0.0093)	1.000 (0.0030)	0.999 (0.0042)	0.955 (0.0266)	1.000 (0.0035)	0.999 (0.0042)	1.000 (0.0030)
	DM	0.751 (0.0515)	0.997 (0.0074)	0.999 (0.0042)	0.999 (0.0051)	0.951 (0.0231)	0.999 (0.0037)	0.999 (0.0051)	0.999 (0.0042)
	ANOVA	0.739 (0.0529)	0.982 (0.0153)	<b>1.000</b> (0.0000)	<b>1.000</b> (0.0000)	0.935 (0.0280)	0.999 (0.0052)	<b>1.000</b> (0.0000)	<b>1.000</b> (0.0000)
	KruskalWallis	0.741 (0.0579)	0.984 (0.0133)	<b>1.000</b> (0.0000)	<b>1.000</b> (0.0000)	0.938 (0.0240)	0.999 (0.0037)	<b>1.000</b> (0.0000)	<b>1.000</b> (0.0000)
	DeSeq2	0.783 (0.0461)	<b>0.999</b> (0.0051)	<b>1.000</b> (0.0000)	<b>1.000</b> (0.0000)	0.731 (0.0606)	0.916 (0.0297)	0.980 (0.0177)	<b>1.000</b> (0.0000)
	edgeR	0.717 (0.0564)	0.987 (0.0127)	0.999 (0.0042)	<b>1.000</b> (0.0000)	0.699 (0.0580)	0.930 (0.0392)	0.977 (0.0169)	<b>1.000</b> (0.0000)
	metagenomeSeq	0.659 (0.0666)	0.996 (0.0082)	0.982 (0.0128)	1.000 (0.0000)	<b>0.746</b> (0.0528)	<b>0.970</b> (0.0238)	0.995 (0.0093)	<b>1.000</b> (0.0000)
ZINB	ZINB-DPP	<b>0.459</b> (0.0582)	<b>0.845</b> (0.0467)	<b>0.912</b> (0.0267)	0.971 (0.0186)	0.716 (0.0514)	0.705 (0.0532)	0.956 (0.0223)	0.986 (0.0142)
	ZINB-TSS	0.403 (0.0651)	0.835 (0.0402)	0.906 (0.0289)	0.969 (0.0167)	0.681 (0.0487)	0.704 (0.0520)	0.954 (0.0216)	0.986 (0.0144)
	ZINB-Q75	0.407 (0.0598)	0.837 (0.0428)	0.906 (0.0314)	<b>0.972</b> (0.0187)	0.676 (0.0559)	0.704 (0.0520)	0.952 (0.0210)	0.985 (0.0157)
	ZINB-RLE	NA (-)	NA (-)	NA (-)	NA (-)	NA (-)	NA (-)	NA (-)	NA (-)
	ZINB-TMM	0.399 (0.0548)	0.832 (0.0448)	0.905 (0.0315)	0.967 (0.0185)	0.674 (0.0551)	0.703 (0.0520)	0.955 (0.0223)	<b>0.987</b> (0.0138)
	ZINB-CSS	0.399 (0.0580)	0.832 (0.0433)	0.904 (0.0292)	0.969 (0.0190)	0.663 (0.0540)	0.703 (0.0522)	0.954 (0.0212)	0.986 (0.0125)
	DM	0.077 (0.0471)	0.327 (0.0553)	0.472 (0.0594)	0.923 (0.0277)	0.217 (0.0689)	0.518 (0.0593)	0.767 (0.0466)	0.957 (0.0243)

Generative Model	Methods	Simulation Setting							
		$K = 2$				$K = 3$			
		$n = 24$		$n = 108$		$n = 24$		$n = 108$	
ZINB	ANOVA	$\sigma = 1$	$\sigma = 2$	$\sigma = 1$	$\sigma = 2$	$\sigma = 1$	$\sigma = 2$	$\sigma = 1$	$\sigma = 2$
		<b>0.099</b> (0.0720)	<b>0.412</b> (0.0847)	<b>0.741</b> (0.0511)	<b>0.930</b> (0.0234)	<b>0.217</b> (0.1070)	<b>0.374</b> (0.0917)	<b>0.870</b> (0.0341)	<b>0.954</b> (0.0271)
	KruskalWallis	<b>0.031</b> (0.0583)	<b>0.122</b> (0.0862)	<b>0.372</b> (0.0689)	<b>0.634</b> (0.0557)	<b>0.007</b> (0.0347)	<b>0.010</b> (0.0392)	<b>0.488</b> (0.0726)	<b>0.795</b> (0.0435)
	DeSeq2	<b>0.223</b> (0.0580)	<b>0.627</b> (0.0672)	<b>0.727</b> (0.0554)	<b>0.963</b> (0.0237)	<b>0.295</b> (0.0685)	<b>0.408</b> (0.0647)	<b>0.643</b> (0.0677)	<b>0.844</b> (0.0420)
	edgeR	NA (-)	NA (-)	NA (-)	NA (-)	NA (-)	NA (-)	NA (-)	NA (-)
	metagenomeSeq	<b>0.072</b> (0.0518)	<b>0.232</b> (0.0598)	<b>0.223</b> (0.0603)	<b>0.672</b> (0.0675)	<b>0.094</b> (0.0506)	<b>0.154</b> (0.0743)	<b>0.186</b> (0.0560)	<b>0.360</b> (0.0625)

**Table 2:** DM and ZINB simulation: Matthews correlation coefficient (MCC) given by all methods. In each cell, the top number is the averaged MCC over 50 independent datasets, and the bottom number in parentheses is the standard error. Result from the model that achieved best performance under the associated scenario (each column) is marked in bold.

,

Real Data Sample Type	Methods	Synthetic Setting							
		AUC				MCC			
		$\sigma = 1$		$\sigma = 2$		$\sigma = 1$		$\sigma = 2$	
		$n = 24$	$n = 108$	$n = 24$	$n = 108$	$n = 24$	$n = 108$	$n = 24$	$n = 108$
Skin	ZINB-DPP	0.908 (0.0303)	0.978 (0.0139)	0.997 (0.0065)	<b>1.000</b> (0.0001)	<b>0.594</b> (0.0856)	<b>0.825</b> (0.0511)	<b>0.963</b> (0.0318)	0.995 (0.0099)
	ZINB-TSS	<b>0.911</b> (0.0314)	0.966 (0.0192)	0.997 (0.0057)	1.000 (0.0006)	0.581 (0.0841)	0.812 (0.0557)	0.961 (0.0358)	0.995 (0.0099)
	ZINB-Q75	0.901 (0.0328)	0.970 (0.0208)	0.997 (0.0075)	1.000 (0.0003)	0.563 (0.0901)	0.817 (0.0538)	0.959 (0.0365)	0.995 (0.0110)
	ZINB-RLE	0.909 (0.0315)	0.965 (0.0222)	0.997 (0.0065)	1.000 (0.0002)	0.593 (0.0858)	0.813 (0.0525)	0.960 (0.0333)	0.995 (0.0099)
	ZINB-TMM	0.907 (0.0290)	0.968 (0.0181)	0.997 (0.0055)	1.000 (0.0004)	0.587 (0.0831)	0.813 (0.0588)	0.958 (0.0354)	<b>0.996</b> (0.0086)
	ZINB-CSS	0.896 (0.0337)	0.971 (0.0176)	0.996 (0.0080)	1.000 (0.0004)	0.549 (0.0958)	0.810 (0.0510)	0.958 (0.0349)	<b>0.996</b> (0.0086)
	DM	0.866 (0.0322)	<b>0.978</b> (0.0090)	<b>0.998</b> (0.0030)	1.000 (0.0003)	0.451 (0.0926)	0.795 (0.0512)	0.959 (0.0326)	0.993 (0.0110)
	ANOVA	0.810 (0.0656)	0.940 (0.0293)	0.985 (0.0169)	0.999 (0.0015)	0.555 (0.0905)	0.722 (0.0705)	0.888 (0.0468)	0.982 (0.0178)
	KruskalWallis	0.800 (0.0676)	0.960 (0.0199)	0.989 (0.0142)	1.000 (0.0003)	0.546 (0.0872)	0.766 (0.0638)	0.903 (0.0528)	0.996 (0.0083)
	DeSeq2	0.733 (0.0621)	0.841 (0.0546)	0.975 (0.0224)	0.995 (0.0082)	0.474 (0.0783)	0.705 (0.0721)	0.939 (0.0424)	0.982 (0.0220)
	edgeR	0.724 (0.0705)	0.914 (0.0390)	0.978 (0.0194)	0.998 (0.0057)	0.429 (0.1483)	0.661 (0.0916)	0.882 (0.0736)	0.982 (0.0220)
	metagenomeSeq	0.687 (0.1089)	0.828 (0.0888)	0.968 (0.0457)	0.956 (0.0805)	0.364 (0.1246)	0.570 (0.1121)	0.862 (0.0966)	0.980 (0.0279)
	Feces	ZINB-DPP	0.902 (0.0334)	0.911 (0.0380)	0.991 (0.0103)	0.994 (0.0069)	0.585 (0.0972)	<b>0.674</b> (0.0877)	<b>0.937</b> (0.0459)
ZINB-TSS		0.902 (0.0320)	0.885 (0.0444)	0.991 (0.0109)	0.989 (0.0123)	0.598 (0.1014)	0.659 (0.0949)	0.933 (0.0506)	0.926 (0.0471)
ZINB-Q75		0.858 (0.0753)	0.882 (0.0443)	0.987 (0.0181)	0.988 (0.0122)	0.512 (0.1080)	0.664 (0.0943)	0.920 (0.0622)	0.923 (0.0476)
ZINB-RLE		<b>0.904</b> (0.0334)	0.878 (0.0425)	0.991 (0.0122)	0.987 (0.0147)	<b>0.605</b> (0.0975)	0.657 (0.0938)	0.927 (0.0498)	0.925 (0.0434)
ZINB-TMM		0.903 (0.0342)	0.886 (0.0379)	0.991 (0.0122)	0.989 (0.0129)	0.604 (0.0898)	0.654 (0.0954)	0.933 (0.0503)	0.926 (0.0406)
ZINB-CSS		0.875 (0.0504)	0.888 (0.0424)	0.990 (0.0138)	0.991 (0.0104)	0.538 0.0960	0.649 0.0926	0.928 0.0456	0.928 0.0416
DM		0.846 (0.0439)	<b>0.933</b> (0.0235)	<b>0.995</b> (0.0075)	<b>0.998</b> (0.0024)	0.423 (0.0834)	0.661 (0.0776)	0.929 (0.0497)	<b>0.955</b> 0.0267



Real Data Sample Type	Methods	Synthetic Setting							
		AUC				MCC			
		$\sigma = 1$		$\sigma = 2$		$\sigma = 1$		$\sigma = 2$	
		$n = 24$	$n = 108$	$n = 24$	$n = 108$	$n = 24$	$n = 108$	$n = 24$	$n = 108$
Feces	ANOVA	0.804 (0.0566)	0.869 (0.0414)	0.977 (0.0205)	0.989 (0.0118)	0.558 (0.1073)	0.605 (0.0802)	0.861 (0.0581)	0.909 (0.0389)
	KruskalWallis	0.805 (0.0548)	0.891 (0.0386)	0.976 (0.0229)	0.996 (0.0070)	0.548 (0.1105)	0.638 (0.0903)	0.865 (0.0592)	0.940 (0.0351)
	DeSeq2	0.732 (0.0738)	0.740 (0.0629)	0.952 (0.0327)	0.933 (0.0320)	0.420 (0.1657)	0.624 (0.0810)	0.918 (0.0557)	0.890 (0.0665)
	edgeR	0.728 (0.0729)	0.829 (0.0488)	0.957 (0.0336)	0.980 (0.0189)	0.390 (0.1417)	0.530 (0.0948)	0.807 (0.0965)	0.894 (0.0549)
	metagenomeSeq	0.607 (0.0642)	0.600 (0.0465)	0.737 (0.0568)	0.711 (0.0237)	0.084 (0.0807)	0.049 (0.0628)	0.203 (0.1577)	0.150 (0.0857)

**Table 3:** Synthetic data: area under the curve (AUC) and Matthews correlation coefficient (MCC) given by all methods. In each cell, the top number is the averaged AUC (or MCC) over 50 independent datasets, and the bottom number in parentheses is the standard error. Result from the model that achieved best performance under the associated scenario (each column) is marked in bold.

**Table 4:** Sensitivity Analysis: AUC and the corresponding standard error (in parenthesis) for different choice of hyperparameters

$b_k$	0.1			1			2			10		
	1	10	100	1	10	100	1	10	100	1	10	100
$h_k$												
$K = 2$ $n = 24$	0.887 (0.0309)	0.888 (0.0253)	0.879 (0.0239)	0.888 (0.0244)	0.878 (0.0258)	0.869 (0.0243)	0.871 (0.0261)	0.858 (0.0290)	0.846 (0.0268)	0.739 (0.0354)	0.730 (0.0336)	0.711 (0.0421)
$K = 2$ $n = 108$	0.987 (0.0127)	0.986 (0.0136)	0.981 (0.0184)	0.996 (0.0057)	0.994 (0.0064)	0.993 (0.0069)	0.996 (0.0046)	0.996 (0.0051)	0.995 (0.0052)	0.967 (0.0098)	0.964 (0.0148)	0.946 (0.0193)
$K = 3$ $n = 24$	0.780 (0.0562)	0.785 (0.0577)	0.783 (0.0589)	0.787 (0.0581)	0.784 (0.0569)	0.792 (0.0542)	0.785 (0.0576)	0.783 (0.0563)	0.793 (0.0503)	0.722 (0.0549)	0.706 (0.0511)	0.675 (0.0438)
$K = 3$ $n = 108$	0.992 (0.0104)	0.991 (0.0110)	0.983 (0.0163)	0.998 (0.0062)	0.997 (0.0067)	0.996 (0.0063)	0.998 (0.0053)	0.998 (0.0047)	0.997 (0.0057)	0.994 (0.0058)	0.986 (0.0103)	0.936 (0.0279)